ORGANOMETALLICS

pubs.acs.org/Organometallics Article

Slicing the π in Three Unequal Pieces: Iridium Complexes with Alkyne, Iminoxolene, and Dioxolene Ligands

David A. Haungs and Seth N. Brown*



Cite This: Organometallics 2022, 41, 3612-3626



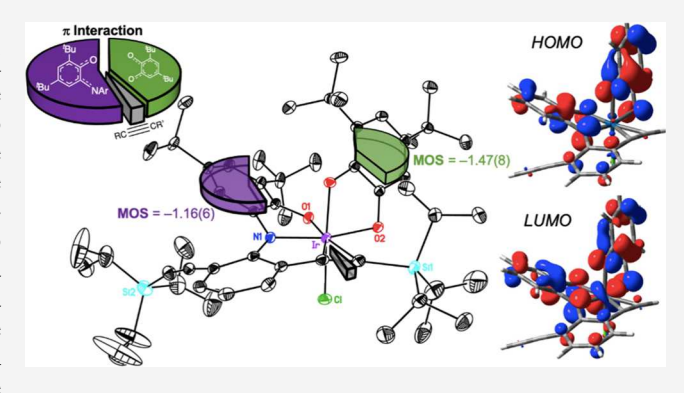
ACCESS I

III Metrics & More

Article Recommendations

Supporting Information

ABSTRACT: The formally isoelectronic alkyne, iminoquinone, and benzoquinone ligands can all exhibit significant metal—ligand π bonding. Condensation of 2,6-bis(triisopropylsilylethynyl)aniline with 3,5-di-*tert*-butyl-1,2-benzoquinone affords a ligand with two such moieties, the alkyne-containing iminoquinone Tipsi. All three groups are installed around a single iridium center by successive treatment of $[(coe)_2IrCl]_2$ with Tipsi and 3,5-di-*tert*-butyl-1,2-benzoquinone to give $(\kappa^2,\eta^2$ -Tipsi)(3,5- t Bu₂Cat)IrCl in two isomeric forms with cis iminoxolene and dioxolene groups and a bound alkyne. Structural, spectroscopic, and computational data indicate that the dioxolene and especially the iminoxolene are strongly engaged in π bonding but that the alkyne is not an effective π donor or acceptor. Pyridine displaces the bound alkyne



in $(\kappa^2,\eta^2\text{-Tipsi})(3,5\text{-}^t\text{Bu}_2\text{Cat})\text{IrCl}$ to give two isomers of $(\kappa^2\text{-Tipsi})(3,5\text{-}^t\text{Bu}_2\text{Cat})\text{Ir}(py)\text{Cl}$, both with the iminoxolene and dioxolene trans to each other. The reaction rates and modest stereospecificity of the dissociative substitution reaction are consistent with a mechanism with competitive, stereochemically distinct, pathways for forming square pyramidal intermediates, which rapidly isomerize to the *trans* isomer before irreversible trapping by pyridine. The five-coordinate intermediates funnel down to the *trans* isomer because it is stabilized by an additional metal–ligand π interaction that is not possible in the *cis* isomers.

■ INTRODUCTION

Pi interactions are well established as important in metalligand bonding in inorganic and organometallic compounds. Conventionally, π ligands are categorized as π -donor ligands, such as oxo or imido ligands, or as π acceptors, such as carbonyls or alkenes. Some ligands may have both π donor and π acceptor characters. For example, the alkyne ligand can accept electrons into one of its π^* orbitals while donating a pair of electrons from a perpendicular π bonding orbital. Given the highly covalent nature of most metal-ligand π interactions, the distinctions between the π donor and π acceptor can sometimes be more formal than real. For example, if the imido group (NR) is considered as a neutral group rather than as a dianion, then it is formally isoelectronic with an alkyne ligand. This relationship is highlighted by the preparation of a complete series of analogous rhenium complexes (ArN)₃ReCl, (ArN)₂(RC≡CR)ReX, (ArN)- $(RC \equiv CR)_2 ReX_1^2$ and $(RC \equiv CR)_3 ReCl^3$ (Ar = 2,6-diisopropylphenyl). Beyond such formal comparisons, it remains important to analyze the real differences in π bonding, such as the strength and polarization of the bonds and their effects on structure and reactivity, among different ligands.

One appealing way of analyzing these bonding issues is to compare different types of π bonding ligands within a single complex. Iminoxolenes and dioxolenes, ligands that can assume a continuum of oxidation states from fully oxidized

(iminoquinone and benzoquinone, respectively) to fully reduced (amidophenoxide and catecholate, respectively), are particularly good candidates for comparison. The π bonding in these ligands involves their so-called redox-active orbitals 4-6 (RAO, shown in the B_2 symmetry dioxolene interaction in Figure 1). The RAOs are unusually high in energy for oxygen or nitrogen lone pairs because of a π^* interaction between the in-phase combination of the heteroatom lone pairs and the filled benzene π orbital. This places their energies close to the energies of the metal $d\pi$ orbitals, fostering strong interactions. Analysis of the intraligand bond distances can be used to give metrical oxidation state (MOS) values, which report on the population of the RAO localized on the ligand, thus offering a means of quantifying the extent of the metal-ligand π interactions. A means of quantifying the extent of π electron donation in coordinated alkynes, using the correlation between electron donation and 13C chemical shift, is also well established.8 However, structural data for complexes contain-

Received: August 26, 2022 Published: November 8, 2022





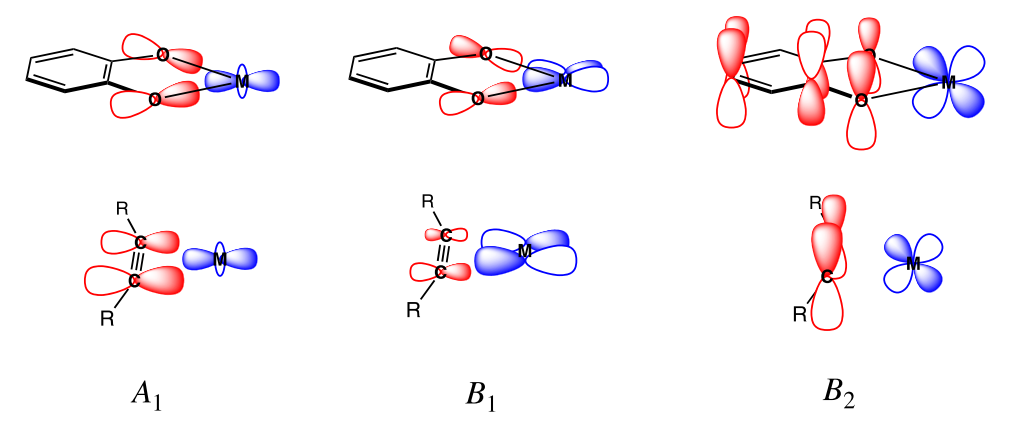


Figure 1. Orbital interactions between metals and dioxolene and alkyne ligands.

ing multiple classes among iminoxolenes, dioxolenes, and alkynes are scarce. A few compounds contain both dioxolene and iminoxolene ligands, 9-12 but the only compound of which we are aware with an alkyne and an iminoxolene or dioxolene ligand is inapposite because it contains bridging rather than terminal catecholates. 13

Here, we describe the preparation of a new iminoxolene ligand that contains silylacetylene groups in the 2,6-positions of the N-aryl substituent. This ligand can be metalated to form an iridium complex with a π bonding network containing iminoxolene, dioxolene, and alkyne ligands. The distribution of π bonding in this complex is illuminated both by structural and spectroscopic measurements, as well as by its effects on the mechanism of substitution of the alkyne group by pyridine.

RESULTS AND DISCUSSION

Synthesis and Characterization of a Mixed Iminoxolene-Dioxolene-Alkyne Complex. The dialkynylated iminoquinone ligand Tipsi (N-(2,6-bis-(triisopropylsilylethynyl)phenyl)-4,6-di-tert-butyl-2-imino-obenzoquinone) is prepared in two steps (Scheme 1). The

Scheme 1. Synthesis of Tipsi

alkynyl groups are installed by Sonogashira coupling of (triisopropysilyl)acetylene with 2,6-dibromoaniline. Subsequent condensation of the substituted aniline with 3,5-di-tertbutyl-1,2-benzoquinone affords the desired iminoquinone. In contrast to such condensations with 2,6-dialkylanilines, which proceed readily at room temperature in the presence of catalytic amounts of carboxylic acids, the dialkynylaniline requires prolonged heating with excess quinone in glacial acetic acid in order to give reasonable conversions to the iminoquinone. This is likely due to the greater electronwithdrawing character of the alkynyl groups (with their more electronegative sp-hybridized carbon atoms) compared to alkyl groups. The iminoquinone is observed to be a mixture of E (major) and E (minor) isomers in solution, as has been previously observed for other iminoquinones.

Tipsi reacts with the bis(cyclooctene)iridium(I) chloride dimer upon heating to give a product with one iminoxolene

and one bound cyclooctene per iridium (Scheme 2). This intermediate is tentatively identified as square planar (Tipsi)-IrCl(coe) based on its symmetry as judged by its ¹H NMR spectrum. This behavior contrasts with that of the iminoquinone Diso (*N*-(2,6-diisopropylphenyl)-4,6-di-*tert*-butyl-2-imino-*o*-benzoquinone), which produces the bis-(iminoquinone) complex (Diso)₂IrCl, ¹⁸ although traces of an analogous mono-ligated species can be observed in the metalation of Diso at very short times before binding of a second Diso ligand takes place.

The monoligated (Tipsi)IrCl(coe) has not been isolated, but if a solution of the compound generated in situ is treated with 3,5-di-*tert*-butyl-o-benzoquinone, two isomers of a mixed-ligand adduct (Tipsi)(3,5- t Bu₂Cat)IrCl (1a-b) form within ten minutes at room temperature (Scheme 2). Initially, isomer 1b predominates (11:1 ratio, Figure S4), but the two equilibrate over the course of several days at room temperature to give a mixture that heavily favors isomer 1a ($K_{eq} = 13.8$ at 21.5 $^\circ$ C in C_6D_6). The compounds are air-stable and 1a is isolated isomerically pure after filtration through silica gel and washing with methanol.

The solid-state structure of 1a (Figure 2, Table 1) shows that the compound is octahedral, with one alkyne of the Tipsi ligand bound in an η^2 fashion, such that Tipsi acts as a tridentate ligand with a *mer* geometry. The free (triisopropylsilyl)ethynyl substituent of Tipsi and the iminoxolene ring twist past each other to minimize steric interference.

Crystallography establishes that the thermodynamically preferred isomer 1a has its di-tert-butyldioxolene ligand oriented such that the oxygen ortho and para to the tertbutyl groups is trans to chloride. The kinetically preferred isomer 1b is assigned as having the same overall geometry as 1a, but with the opposite orientation of the dioxolene ligand (oxygen meta to the tert-butyl groups trans to chloride) based on the negligible changes in the optical spectrum when 1b isomerizes to 1a (Figure S29). Were the central chromophore different in the two isomers, significant changes in the optical spectrum would be expected, as seen for example in previous examples of cis- and trans-bis(iminoxolene)4,18 or -bis-(dioxolene)¹⁹ metal complexes. In principle, the alkyne could be free in 1b and the compound could adopt a five-coordinate, square pyramidal structure analogous to that observed for the bis(iminoxolene) complex (Diso)₂IrCl. This seems unlikely because a change in the coordination number (and geometry) would also be expected to produce substantial changes in the optical spectrum as well. ¹³C NMR spectroscopy confirms that

Scheme 2. Synthesis of (Tipsi)(3,5-^tBu₂Cat)IrCl (1a)

$$[(coe)_2|rCl]_2 \xrightarrow{P_{r_3}Si} \\ Si^P_{r_3}Si \\ 24 \text{ h, } 61 ^{\circ}C$$

$$[bu \\ P_{r_3}Si \\ P_$$

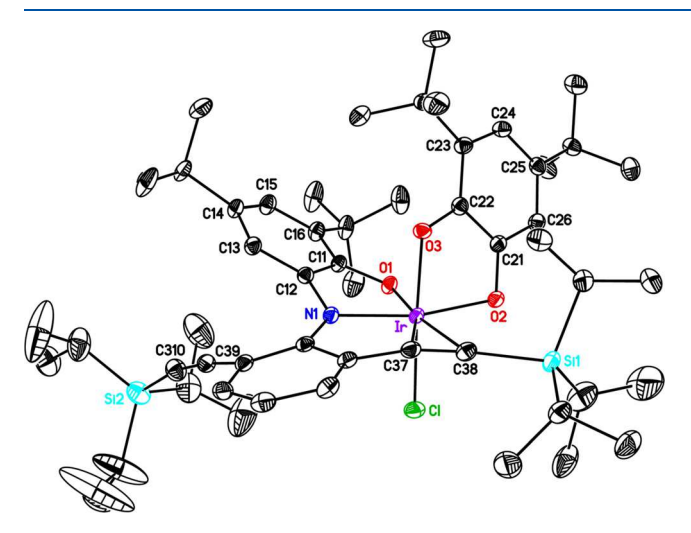


Figure 2. Thermal ellipsoid plot of $(\kappa^2, \eta^2\text{-Tipsi})(3, 5^t\text{Bu}_2\text{Cat})\text{IrCl} \bullet \text{CH}_3\text{OH}$. Hydrogen atoms and solvents are omitted for clarity.

both 1a and 1b contain bound alkynes. In particular, each compound shows one alkynyl signal at a distinctive chemical shift (δ 76.4 for 1a and δ 77.3 for 1b); the signal in 1a is confirmed to be the alkyne carbon bonded to the triisopropylsilyl group on the basis of its long-range coupling to an isopropyl methine proton in the ¹H-¹³C HMBC spectrum (Figures S10, S11, and S15). These peaks are shifted significantly upfield relative to the corresponding carbons in free Tipsi (δ 96.1, 94.7 for the E and Z isomers, respectively) or the other silvlated alkynyl carbon in 1a (δ 101.81). Moderate upfield shifts in the ¹³C NMR spectrum are typical of iridium alkyne complexes. ^{20–24} We tentatively ascribe the greater thermodynamic stability of 1a to the positioning of its dioxolene ligand with its more electron-rich oxygen atom (ortho and para to tert-butyl) trans to the weakly donating chloride, while in 1b, the more electron-rich oxygen atom is trans to the more strongly donating nitrogen.

Structure and Bonding in $(\kappa^2, \eta^2$ -Tipsi)(3,5- t Bu₂Cat)-IrCl. Complex 1a contains cis iminoxolene and dioxolene ligands, with one neutral donor (alkyne) and one uninegative ligand (chloride). As such, it is isoelectronic to group 8 complexes containing two neutral ligands and either two cis iminoxolenes (such as $M(L_{N,O,S})_2^{2.5}$) or two cis dioxolenes

(such as Ru(bpy)(dioxolene)₂²⁶) and is expected to have a similar electronic structure. This is borne out by DFT calculations. In particular, the compound's lowest unoccupied molecular orbital (LUMO) (Figure 3a) is metal-ligand π^* in character and shows significant contributions from the metal as well as both the iminoxolene and dioxolene ligands. The highest occupied molecular orbital (HOMO) is nominally π^* as well, but as has been described previously, the iminoxolene and dioxolene ligands fold in such a way as to minimize the overlap between the metal $d\pi$ orbital and the ligand redoxactive orbitals.⁴ In $(\kappa^2, \eta^2$ -Tipsi)(3,5- t Bu₂Cat)IrCl (1a), the dihedral angles displayed by the iminoxolene (Cl-Ir-N1-C12) of 116.5° (114.3° by DFT) and by the dioxolene (using the alkyne centroid as the first atom) of 117.3° (112.0° by DFT) are similar to values previously observed for isoelectronic group 8 compounds. 4,25,26 Like those compounds, the calculated HOMO of 1a (Figure 3b) is therefore essentially nonbonding and localized on the iminoxolene and dioxolene ligands. In 1a, the preference for obtuse dihedral angles is likely linked to the fact that the atropisomer of the Tipsi ligand with the free alkyne syn to chlorine is observed. Computationally, the atropisomer with the free alkyne anti to chlorine (1') is found to have an iminoxolene dihedral angle of 73.9° and is 3.7 kcal mol⁻¹ higher in energy than the observed structure.

The MOS⁷ derived from intraligand bond lengths (Table 2) of the iminoxolene in 1a is -1.16(6) and of the dioxolene ligand is -1.47(8). Values determined from the DFT-optimized structure are similar. These MOS values are consistent with significant covalency in the π bonds between iridium and both the iminoxolene and dioxolene ligands. A useful way to parse the numerical values is in terms of the π bond order between the metal and the ligand. If the π bond order is zero and the bonding and nonbonding orbitals are filled (as is typically the case), the ligand appears to be fully reduced (MOS = -2.00). The apparent oxidation state increases linearly with the π bond order, with the degree of increase dependent on the polarization of the bonding orbital toward the ligand or the metal.⁵

To interpret the MOS values in terms of the π bond order, one must therefore calibrate the sensitivity of MOS to bond order using compounds of known bond order. For iridium iminoxolenes, (Diso)₂IrCl and (Diso)₂IrI, which have the same nominal oxidation state as (Tipsi)(3,5- t Bu₂Cat)IrCl, afford

Table 1. Summary of Crystal Data for $(\kappa^2, \eta^2$ -Tipsi)(3,5- t BuCat)IrCl • CH₃OH (1a • CH₃OH) and $(\kappa^2$ -Tipsi)(3,5- t BuCat)Ir(py)Cl • PhCH₃ • 0.5 CH₃OH (2b • PhCH₃ • 0.5 CH₃OH) CH₃OH)

	$(\kappa^2, \eta^2$ -Tipsi)(3,5- ^t BuCat)IrCl • CH ₃ OH (1a • CH ₃ OH)	$(\kappa^2\text{-Tipsi})(3,5\text{-}^t\text{BuCat})\text{Ir}(\text{py})\text{Cl} \bullet \text{PhCH}_3 \bullet 0.5 \text{ CH}_3\text{OH} (2b \bullet \text{PhCH}_3 \bullet 0.5 \text{ CH}_3\text{OH})$	
molecular formula	$C_{57}H_{89}ClIrNO_4Si_2$	$C_{68.5}H_{100}CIIrN_2O_{3.5}Si_2$	
formula mass	1136.12	1291.33	
T (K)	120(2)	120(2)	
crystal system	monoclinic	monoclinic	
space group	$P2_1/c$	$P2_1/n$	
λ (Å)	0.71073 Å (Mo Kα)	0.71073 Å (Mo Kα)	
total data	132,715	446,666	
indep refls	14,500	34,182	
$R_{ m int}$	0.0371	0.0887	
obsd refls $[I > 2\sigma(I)]$	13,494	26,654	
a (Å)	10.2405(6)	25.5523(13)	
b (Å)	29.5993(18)	20.3729(11)	
c (Å)	19.2895(15)	28.5372(15)	
α (°)	90	90	
β (°)	94.6612(14)	112.1996(17)	
γ (°)	90	90	
$V(Å^3)$	5827.5(7)	13754.5(13)	
Z	4	8	
$\mu \text{ (mm}^{-1})$	2.420	2.059	
crystal size (mm)	$0.27 \times 0.28 \times 0.29$	$0.21 \times 0.16 \times 0.14$	
refined params	596	1450	
R1, wR2 $[I > 2\sigma(I)]$	0.0364, 0.0762	0.0435, 0.0839	
R1, wR2 [all data]	0.0396, 0.0774	0.0653, 0.0913	
goodness of fit	1.282	1.032	

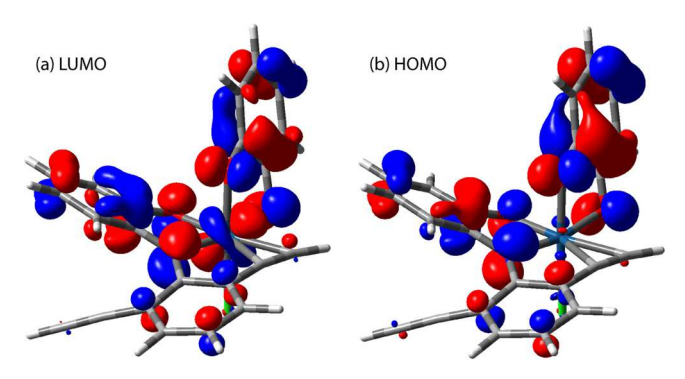


Figure 3. Frontier Kohn–Sham orbitals of $(\kappa^2, \eta^2$ -Tipsi)(Cat)IrCl (1), with triisopropylsilyl and *tert*-butyl groups in **1a-b** replaced with hydrogen. (a) LUMO; (b) HOMO.

Table 2. Selected Distances (Å) and MOS⁷ for $(\kappa^2, \eta^2$ -Tipsi)(3,5- tBu_2Cat)IrCl (1a) and $(\kappa^2$ -Tipsi)(3,5- tBu_2Cat)Ir(py)Cl (2b)^a

	$(\kappa^2, \eta^2$ -Tipsi) (3,5- t Bu ₂ Cat)IrCl (1a)		(κ²-Tipsi)(3,5- ^t Bu ₂ Cat) Ir(py)Cl (2b)	
	X-ray	DFT	X-ray ^b	DFT
Ir-N1	1.986(3)	2.012	1.988(6)	2.023
Ir-O1	1.999(2)	2.024	2.012(14)	2.035
Ir-O2	2.026(2)	2.057	1.999(2)	2.031
Ir-O3	2.007(2)	2.041	1.997(7)	2.029
Ir-Cl	2.3367(8)	2.375	2.3190(15)	2.364
Ir-C37	2.170(3)	2.218		
Ir-C38	2.271(3)	2.265		
Ir-N2			2.072(3)	2.131
O1-C11	1.316(4)	1.310	1.311(4)	1.306
N1-C12	1.368(4)	1.370	1.350(4)	1.359
C11-C12	1.436(4)	1.447	1.427(7)	1.443
C12-C13	1.412(4)	1.416	1.418(5)	1.419
C13-C14	1.369(4)	1.380	1.366(5)	1.378
C14-C15	1.433(4)	1.419	1.428(5)	1.420
C15-C16	1.379(4)	1.379	1.374(7)	1.381
C16-C11	1.420(4)	1.414	1.426(6)	1.413
O2-C21	1.329(4)	1.313	1.329(4)	1.323
O3-C22	1.329(4)	1.319	1.324(5)	1.319
C21-C22	1.431(4)	1.447	1.411(7)	1.436
C22-C23	1.425(4)	1.411	1.416(14)	1.410
C23-C24	1.383(4)	1.383	1.378(7)	1.386
C24-C25	1.422(4)	1.419	1.414(7)	1.414
C25-C26	1.379(5)	1.382	1.376(7)	1.387
C26-C21	1.393(4)	1.414	1.410(16)	1.408
C37-C38	1.233(5)	1.239	1.200(8)	1.210
C39-C310	1.202(5)	1.210	1.196(6)	1.208
iminoxolene MOS	-1.16(6)	-1.18(7)	-1.08(6)	-1.12(6)
dioxolene MOS	-1.47(8)	-1.32(7)	-1.56(10)	-1.45(5)

"Values in the Roman type are measured crystallographically; values in *italics* are from DFT calculations (B3LYP, SDD basis set for Ir and 6-31G* basis set for other atoms) on complexes with all *tert*-butyl and triisopropylsilyl groups replaced with hydrogen atoms. ^bMetrical data are averaged among chemically equivalent values, with stated esds reflecting both the variance in the measured values and the statistical uncertainty of the crystallographic model.

useful calibration points. Given the MOS values of -1.27(8) and -1.32(11), respectively, in the bis(iminoxolenes), ¹⁸ with π bond orders of approximately 0.5, the bonding orbital can be estimated to be approximately 70% metal-centered. It is more

difficult to find a good iridium dioxolene comparison to compound ${\bf 1a}$, as the only reported iridium bis(dioxolene) structure is that of $(3,6^{-t}{\bf Bu_2Cat})_2{\rm Ir}({\rm cod}),^{27}$ which is overall one electron more reduced than ${\bf 1a}$. This electron occupies a metal-dioxolene π^* orbital, giving a π bond order of 0.25, which means that the MOS of -1.66(12) in this complex translates to a bonding orbital that is 68% metal-centered, very similar to the iminoxolenes. Using these calibrations to assess the π bonding in ${\bf 1a}$ gives a π bond order of 0.60 for the iminoxolene-iridium bond and 0.39 for the π bond order of the dioxolene-iridium bond.

These values are consistent with the appearance of the calculated frontier orbitals of 1 (Figure 3): Both the iminoxolene and dioxolene RAOs are substantial contributors to both the HOMO (π bonding) and LUMO (π^*), but the dioxolene orbitals are slightly greater contributors to the former and the iminoxolene orbitals to the latter. The overall picture is that the total amount of π bonding from the iminoxolene/dioxolene ligand set is very similar to the bis(iminoxolene) ligand set in (Diso)₂IrX, as judged, for example, by the total MOS values (-2.63 for 1a vs -2.59 for (Diso)₂IrX), but with the bonding modestly skewed toward greater participation of the iminoxolene over the dioxolene.

The effect of replacing iminoxolenes with dioxolenes has also been studied in molybdenum complexes. For example, the iminoxolenes in the seven-coordinate tris(iminoxolene)molybdenum complex (MeClamp)Mo²⁸ have an average MOS value of -1.52(9), which shifts to -1.30(9) in the seven-coordinate bis(iminoxolene)-monocatecholate complex (*BuClip)Mo-(3,5-^tBu₂Cat)(py).²⁹ As in the iridium complexes, the iminoxolene/dioxolene substitution appears to have little effect on the overall degree of π bonding (the MOS values of the three redox-active ligands in both Mo complexes sum to -4.56) as the iminoxolenes take on a larger share of the π bonding. Curiously, this pattern is not observed in sixcoordinate molybdenum complexes; the average iminoxolene MOS in octahedral tris(iminoxolene) complexes $(-1.64)^{17}$ is indistinguishable from that observed in the bis(iminoxolene)monocatecholate complex ('BuClip)Mo(3,5-'Bu₂Cat) $(-1.66)^9$

What role does the alkyne play in the π bonding of compound 1? Spectroscopic, structural, and computational data indicate that the η^2 -alkyne plays a negligible role as either a π -donor or a π -acceptor. Four-electron donor alkyne complexes of iridium are known, 30 and, as documented in group 6 complexes,^{1,8} the key spectroscopic signature of π donation is a downfield shift in the ¹³C NMR.³¹ For example, in (PhB[CH₂PPh₂]₃)Ir(PhCCH), the alkyne carbons of the four-electron donor alkyne resonate at δ 179.8 and 166.3 ppm, while in the PMe₃ adduct (PhB[CH₂PPh₂]₃)Ir(PhCCH)-(PMe₃), where π donation from the alkyne is precluded, the resonances shift upfield to δ 89.0 and 83.1 ppm. The alkyne resonances of 1a (δ 76.4, 102 ppm) are most consistent with an insignificant amount of π donation. Structurally, π donation from the alkyne results in characteristically short metal-carbon distances (typically 2.02 Å for four-electron donor alkynes to iridium). 31,32 The observed distances of 2.170(3) and 2.271(3) Å in 1a are not only much too long to be consistent with significant π donation, they are on the long end of known iridium-alkyne distances even in two-electron donor alkynes, which are typically in the range of 2.08-2.14 Å. 23,33 The only similar iridium-carbon distances in bonds to simple alkynes are in the cationic Ir(III) complex $[Cp*Ir(P^C)(PhCCMe)]$ -

Scheme 3. Pyridine Addition to $(\kappa^2, \eta^2\text{-Tipsi})(3,5\text{-}^t\text{Bu}_2\text{Cat})\text{IrCl }(1a-b)$ To Generate $(\kappa^2\text{-Tipsi})(3,5\text{-}^t\text{Bu}_2\text{Cat})\text{Ir}(py)\text{Cl }(2a-b)$ $(C_6D_{6}, 21.5 \, ^{\circ}\text{C})$

BAr_F (P^C = cyclometalated PMe(2,6-Me₂C₆H₃)₂), with Ir–C distances of 2.181(5) and 2.201(5) Å.²⁴ The bulk of the triisopropylsilyl group does not appear to play a major role in the long metal-alkyne bonds in 1a, as DFT calculations on the terminal alkyne analogue show similar distances.

The η^2 -alkyne in **1a** also appears to engage in minimal π backbonding with the iridium center. Here, the most useful spectroscopic handle is the C≡C stretch in the IR spectrum. The frequency of this stretch does not appear to be strongly sensitive to alkyne π donation (for example, it shifts by only 5 cm⁻¹ on the addition of PMe₃ to (PhB[CH₂PPh₂]₃)Ir-(PhCCH)³²) but does tend to shift to lower frequency as the metal becomes more electron-rich. The frequency of the bound alkyne in 1a, 1966 cm⁻¹, is higher than any other iridium-alkyne stretches of which we are aware; only cationic Ir(III) complexes (e.g., $[Cp*Ir(C_3H_5)(PhC \equiv CPh)]OTf$, 1905 cm⁻¹) 20 are similar. Structurally, the C \equiv C distance, which is known to be insensitive to π donation from the alkyne³⁴ but which elongates on increasing backbonding, is minimally perturbed in 1a. The bound alkyne C≡C distance is 1.233(5) Å, only 0.03 Å longer than the free alkyne in 1a, and similar to the bond distances observed in cationic Ir(III) adducts (e.g., [Cp*Ir(P^C)(PhCCMe)]BAr_F, 1.245(10) Å).²⁴

DFT calculations are consistent with the lack of significant π interactions between iridium and the alkyne in 1a. Neither the LUMO nor the HOMO, each of which shows strong participation of the π orbitals on the iminoxolene and dioxolene ligands, has significant alkyne character. Overall, the alkyne is thus seen to be neither a borrower nor a lender of π electrons (Polonius-type alkyne). The lack of significant π backbonding is particularly noteworthy, as it indicates a metal center that is at least as electron-poor as cationic Ir(III). The apparent iridium oxidation state of +3.63 derived from the MOS values of the iminoxolene and dioxolene ligands is thus qualitatively congruent with the electron density at the metal center

Synthesis and Characterization of (Tipsi)-(3,5- t Bu₂Cat)Ir(py)Cl. By substituting the coordinated alkyne in $(\kappa^2,\eta^2$ -Tipsi)(3,5- t Bu₂Cat)IrCl (1a) with a σ -only ligand, we sought to confirm the π -innocence of the alkyne and investigate the stereochemical and mechanistic implications of ligand substitution in the mixed iminoxolene/dioxolene system. To these ends, alkyne adduct 1a was reacted with

pyridine (Scheme 3). Isomer 1a reacts to give two isomers of the pyridine adduct (κ^2 -Tipsi)(3,5- t Bu₂Cat)Ir(py)Cl, 2a and 2b, in a 10.6:1 ratio at 21.5 °C. Isomer 1b reacts with pyridine to form the same two isomers but in a mixture that favors 2b over 2a by a factor of 2.1, as judged by the addition of pyridine in situ to the 1b-enriched kinetic mixture of (Tipsi)-(3,5- t Bu₂Cat)IrCl. In these reactions, the 2a:2b ratio is independent of pyridine concentration. The observation that the ratio does not change over time during the reaction, but is different depending on the precursor, indicates that the product distribution is under kinetic control.

The pyridine adducts 2a and 2b are air- and moisture-stable and can be separated from each other by chromatography on silica gel. The solid-state structure of isomer 2b (Figure 4) shows that the substitution of the alkyne by pyridine is accompanied by a stereochemical change in the orientation of the iminoxolene and dioxolene ligands from cis to trans. In isomer 2b, the tert-butyl groups in the dioxolene ligand are located ortho/para to the oxygen trans to nitrogen. Given that 1a and 1b differ in the dioxolene orientation and that both pyridine adducts 2a and 2b are formed from both isomers of the alkyne adduct, isomer 2a is assigned to the compound with the same stereochemistry at iridium, but with the positions of the tert-butyl groups in the dioxolene meta to the oxygen trans to N. This assignment is supported by the similarity of the optical spectra of 2a and 2b (Figure S25).

The bonding in compounds (Tipsi)(Cat)Ir(py)Cl (2), as elucidated by DFT calculations, is strikingly similar to that shown in the alkyne adduct 1 despite the change in the geometry from cis to trans. The pseudo-B symmetry LUMO consists of a π antibonding combination of the iminoxolene and dioxolene RAOs with the iridium $d\pi$ orbital, while the pseudo-A symmetry HOMO is ligand-centered and nonbonding (Figure 5). The composition of the frontier orbitals of 2, like those of 1, reflect the relative importance of the redoxactive orbitals of the iminoxolene and the dioxolene. Both ligands contribute significantly to both orbitals, but the dioxolene clearly contributes more to the HOMO and the iminoxolene more to the LUMO. This greater involvement of the dioxolene in the filled orbitals is consistent with the MOS values for the two ligands (-1.08(7)) for Tipsi and -1.56(9)for ^tBu₂Cat in 2b).

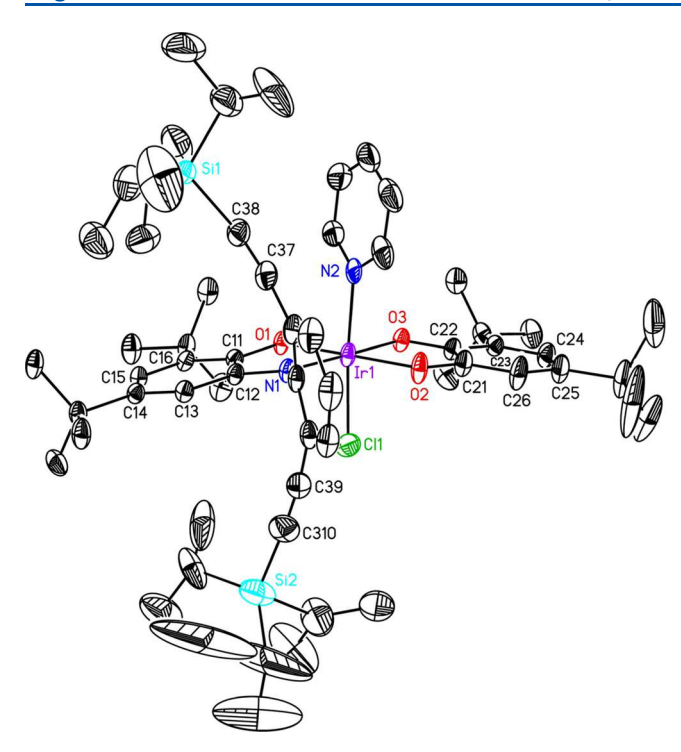


Figure 4. Thermal ellipsoid plot of $(\kappa^2$ -Tipsi)(3,5- t Bu₂Cat)Ir(py)Cl • PhCH₃ • 0.5 CH₃OH. One of the two crystallographically independent molecules is shown, with only the major component of the disordered isopropyl groups. Hydrogen atoms and solvents are omitted for clarity.

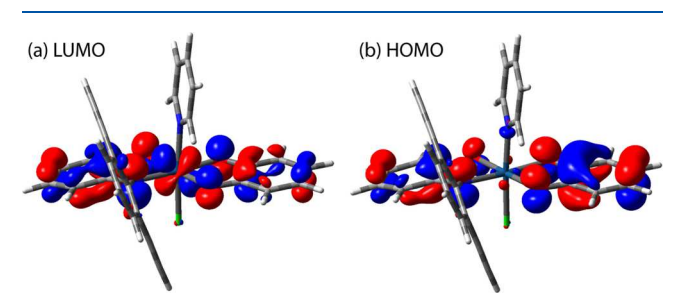


Figure 5. Frontier Kohn–Sham orbitals of (Tipsi)(Cat)Ir(py)Cl (2), with triisopropylsilyl and *tert*-butyl groups in **2a-b** replaced with hydrogen. (a) LUMO; (b) HOMO.

The MOS values in 2b are very similar to those shown by 1a. Previous studies of osmium bis(iminoxolene) complexes have shown that π acceptor ancillary ligands cause a noticeable positive shift in MOS values.⁴ The similarity of the MOS values in 1a and 2b is thus consistent with the characterization of the alkyne as a Polonius-type³⁵ ligand. It is conceivable that the replacement of alkyne by pyridine did significantly affect the electronic structure, if the change in the geometry from cis to trans exerted an opposite effect of comparable magnitude. However, computational MOS values of cis-(Tipsi)(Cat)Ir-(py)Cl and trans-(Tipsi)(Cat)Ir(py)Cl do not differ substantially (dioxolene/iminoxolene of -1.45(5)/-1.12(6) for the trans isomer and an average of -1.47(11)/-1.12(9) for the average of the four possible cis stereoisomers), suggesting that neither the ligand substitution nor the change in the geometry has a large effect on the electronic structure.

Kinetics of Isomerization and Pyridine Addition Reactions of $(\kappa^2, \eta^2\text{-Tipsi})(3,5\text{-}^t\text{Bu}_2\text{Cat})\text{IrCl}$. The stereo-isomerization of 1b to 1a was studied by ^1H NMR in C_6D_6

at 21.5 °C by monitoring the time evolution of the in situgenerated mixture of isomers. The isomerization obeys first-order kinetics with $k_{\rm obs} = 2.05(13) \times 10^{-5} \, {\rm s}^{-1} \, (k_{\rm lisom}$, Figure S30).

Addition of pyridine to isomer **1a** of $(\kappa^2, \eta^2$ -Tipsi)-(3,5-^tBu₂Cat)IrCl was monitored by optical spectroscopy, with clean isosbestic points being observed as the compound is transformed into the mixture of pyridine adduct isomers 2a + 2b (Figure 6). The good adherence of the absorbance vs time data to exponential decay (Figure S31) indicates that the reaction is first order in iridium, and the invariance of the observed first-order rate constant to pyridine concentration (Figure S32) indicates that the reaction order in pyridine is zero. ¹H NMR measurements establish that the ratio of 2a:2b produced in the reaction is also independent of the pyridine concentration. At 21.5 °C, this ratio is 10.7:1, which allows one to partition the overall rate constant $k_{\rm 1a+py} = 2.60(9) \times 10^{-6}$ s⁻¹ into separate rate constants $k_{\rm 1a\to2a}$ and $k_{\rm 1a\to2b}$ for the two pathways (Table 3). Measurement of the overall rate constant for pyridine addition at temperatures from 21.5 to 70 °C gives an Eyring plot (Figure 7) from which activation parameters of $\Delta H^{\ddagger} = 26.6(2)$ kcal mol⁻¹ and $\Delta S^{\ddagger} = 7.1(6)$ cal mol⁻¹ K⁻¹ could be determined. These activation parameters, and the zero-order dependence on the incoming ligand, are consistent with a dissociative mechanism where the alkyne is lost from the adduct 1a in the rate-limiting step of the reaction.

Like isomer 1a, isomer 1b reacts with pyridine to form adducts 2a and 2b, albeit in a ratio much more enriched in 2b (1:2.1 at 21.5 °C). The rate of this process was monitored by optical spectroscopy, starting with the mixture of $(\kappa^2, \eta^2$ -Tipsi)(3,5- 1 Bu₂Cat)IrCl generated in situ (>90% isomer 1b). Pyridine addition to 1b was found to be over 100 times faster than addition to isomer 1a at 21.5 °C (Table 3), and as with the reaction of 1a, neither the observed rate constant nor the ratio of products varies with varying pyridine concentration. Measurement of the rate by 1 H NMR spectroscopy gave indistinguishable results (Figure S34; $k_{1b+py} = 2.77(10) \times 10^{-4} \, \rm s^{-1}$).

Loss of pyridine from the pyridine adduct 2a is observed (by the exchange of pyridine- d_5) at elevated temperatures. At $60.0\,^{\circ}$ C in C_6D_6 , isomer 2a of $(\kappa^2$ -Tipsi)(3,5- t Bu₂Cat)Ir(py)Cl converts to 2a- d_5 in the presence of excess py- d_5 with a rate constant of $k=6.10(7)\times 10^{-5}\,\mathrm{s}^{-1}$. The observed rate constant is independent of the concentration of pyridine- d_5 , consistent with the dissociative mechanism. The barrier for pyridine dissociation is $26.0\,\mathrm{kcal}\,\mathrm{mol}^{-1}$ at 333 K. The replacement of pyridine in 2a proceeds with complete stereoretention, with no detectable formation of 2b over >50 half-lives at $60.0\,^{\circ}$ C. The behavior of isomer 2b is strictly analogous ($k_{\mathrm{diss}}=6.96(4)\times 10^{-5}\,\mathrm{s}^{-1}$ at $60.0\,^{\circ}$ C, $\Delta G^{\ddagger}=25.9\,\mathrm{kcal}\,\mathrm{mol}^{-1}$, no formation of 2a over >50 half-lives).

Mechanism of Isomerization and Pyridine Addition Reactions of $(\kappa^2,\eta^2\text{-Tipsi})(3,5\text{-}^t\text{Bu}_2\text{Cat})\text{IrCl}$. The experimental observations establish that the isomerization equilibrium between isomers 1a and 1b of $(\kappa^2,\eta^2\text{-Tipsi})(3,5\text{-}^t\text{Bu}_2\text{Cat})\text{IrCl}$ must share common intermediates with the pyridine addition to these compounds to give the pyridine adducts 2a and 2b. The kinetics measurements indicate that isomerization of 1b to 1a takes place one-sixteenth as rapidly as the overall rate of pyridine addition to 1b. Therefore, if the two pathways were independent of one another—for example, if the isomerization of the alkyne complex took place by a trigonal twist—then a significant amount of 1a $(\sim 5\%)$ would accumulate by the time

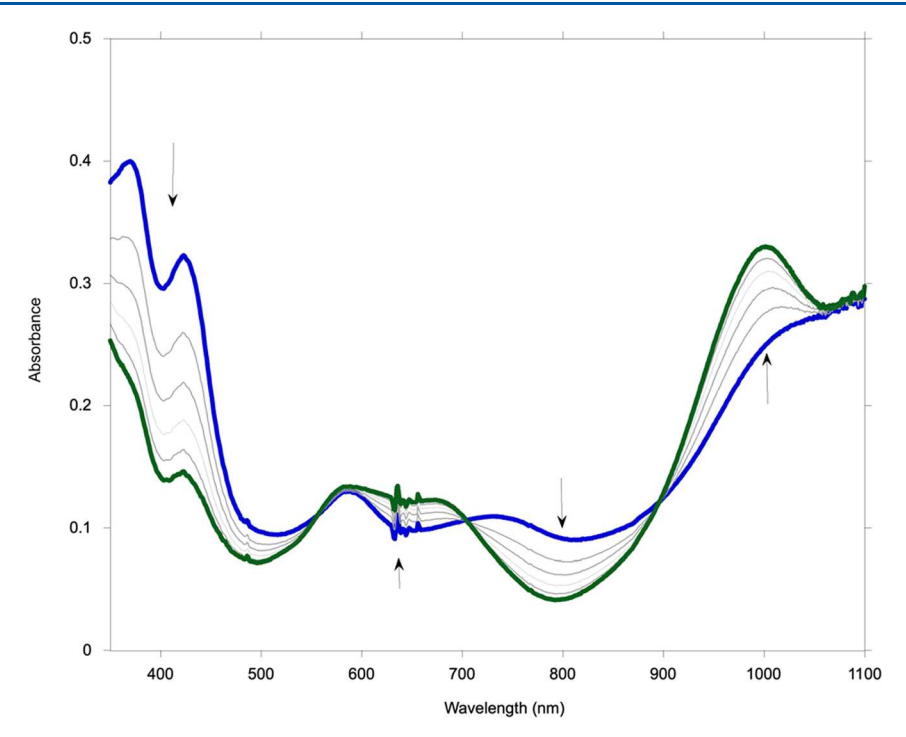


Figure 6. Time evolution of optical spectra in the reaction of $(\kappa^2, \eta^2\text{-Tipsi})(3,5\text{-}^t\text{Bu}_2\text{Cat})\text{IrCl }(1\text{a}, 4.67 \times 10^{-5} \text{ M})$ with pyridine (0.0618 M, C_6H_{6} , 21.5 °C). Traces are shown for scans taken every 30 h, starting when the reaction was initiated (solid blue line) and ending at t = 150 h (solid green line).

Table 3. Measured and Derived Rate Constants, Equilibrium Constants, and Stereoselectivities for Reactions of Both Isomers of $(\kappa^2, \eta^2\text{-Tipsi})(3,5\text{-}^t\text{Bu}_2\text{Cat})\text{IrCl}$ in Benzene at 21.5 °C

quantity	value	source
stereoselectivity of $1a + py: 2a/2b(S_{1a})$	10.7(20)	¹H NMR
stereoselectivity of $1b + py$: $2b/2a(S_{1b})$	2.1(4)	¹H NMR
$K_{1\mathbf{b} \rightleftharpoons 1\mathbf{a}}(K)$	13.8(5)	¹H NMR
$k_{ m 1a+py}$	$2.60(9) \times 10^{-6} \text{ s}^{-1}$	UV-vis
$k_{1\mathbf{b}+\mathrm{py}}$	$3.01(7) \times 10^{-4} \text{ s}^{-1}$	UV-vis
$k_{ m 1isom}$	$2.05(13) \times 10^{-5} \text{ s}^{-1}$	¹H NMR
$k_{1a o 1b}$	$1.39(10) \times 10^{-6} \text{ s}^{-1}$	$k_{1\text{isom}}/(1+K)$
$k_{1a o 2a}$	$2.38(9) \times 10^{-6} \text{ s}^{-1}$	$k_{1a+py}(S_{1a}/(1+S_{1a}))$
$k_{1a o 2b}$	$2.2(4) \times 10^{-7} \text{ s}^{-1}$	$k_{1a+py}/(1 + S_{1a})$
$k_{1\mathbf{b} o 1\mathbf{a}}$	$1.91(12) \times 10^{-5} \text{ s}^{-1}$	$k_{1\text{isom}}K/(1+K)$
$k_{1\mathbf{b} o 2\mathbf{b}}$	$2.04(13) \times 10^{-4} \text{ s}^{-1}$	$k_{1b+py}(S_{1b}/(1+S_{1b}))$
$k_{1b o 2a}$	$9.7(10) \times 10^{-5} \text{ s}^{-1}$	$k_{1b+py}/(1+S_{1b})$

reaction of 1b with pyridine is 95% complete (see derivation A in the SI). NMR monitoring of the reaction of 1b with pyridine indicates that no 1a is formed under these conditions (Figure S7). In other words, addition of pyridine suppresses the 1a/1b isomerization, implying that pyridine captures the intermediates involved in this isomerization.

The reaction order of zero in pyridine indicates that the rate-determining step in pyridine addition proceeds through a transition state that does not contain pyridine. The positive entropy of activation strongly suggests that the formation of the intermediate in the reaction involves dissociation of the alkyne ligand rather than, say, a rearrangement of a six-coordinate species. The trans stereochemistry of the observed pyridine adducts 2 implies that their five-coordinate precursors 3 must likewise have trans stereochemistry. The fact that the stereoselectivity of the reactions to form 2a and 2b from either 1a or 1b is independent of pyridine concentration implies that any steps preceding formation of 3 from 1 do not

involve pyridine addition or loss, and that once formed, five-coordinate intermediates 3 react rapidly with pyridine.

If intermediates 3 are the key intermediates in interconverting 1a and 1b, then the reaction landscape relating the isomers of 1 and 3 can be constructed using only the data from the kinetics and stereoselectivity of reactions of 1a and 1b with pyridine and from the equilibrium between 1b and 1a, $K_{1b\rightleftharpoons 1a}$ (Figure 8). Interconverting 1a and 1b requires that exactly one of the steps of dissociating the alkyne to form intermediate 3 and having it re-bind adduct 1 involves changing the stereochemistry from a to b or vice versa. There are thus two inequivalent pathways for the isomerization ($1a \rightleftharpoons 3b \rightleftharpoons$ 1b and $1a \rightleftharpoons 3a \rightleftharpoons 1b$), with the lower overall barrier associated with the latter pathway, which accounts for 88% of the isomerization rate at 21.5 °C. Overall, the reactivity with pyridine and the overall isomerization equilibrium allow one to predict a value for $k_{1\text{isom}} = 3.0(2) \times 10^{-5} \text{ s}^{-1}$ (see derivation B in the SI). The reasonable agreement of this prediction with

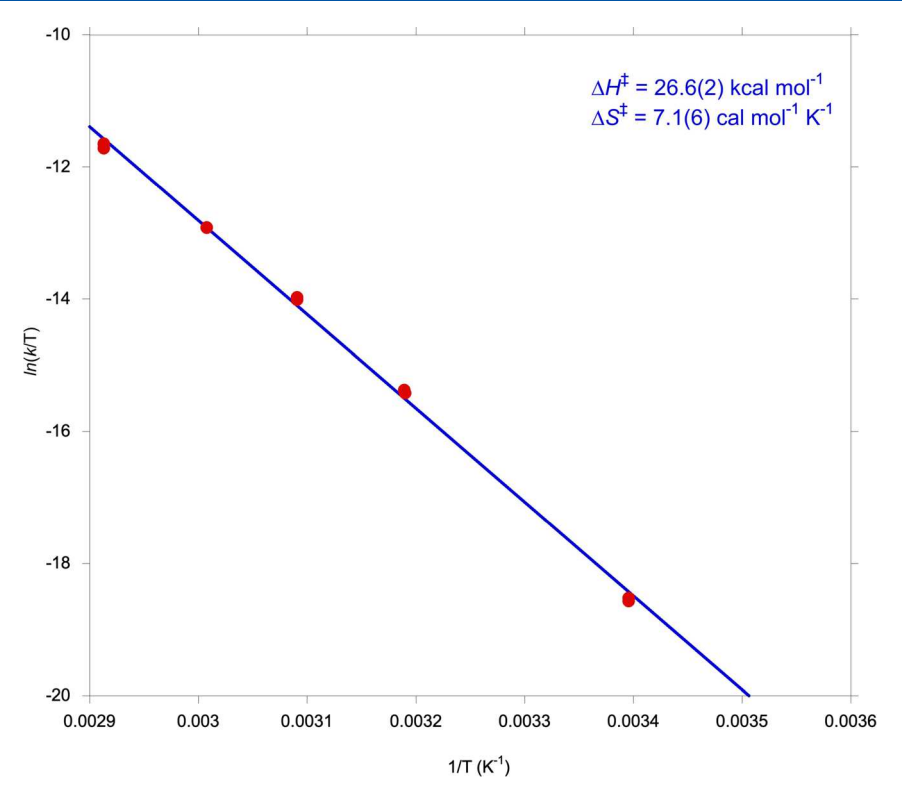


Figure 7. Eyring plot for the reaction of $(\kappa^2, \eta^2$ -Tipsi)(3,5- t Bu₂Cat)IrCl (isomer 1a) with pyridine (C₆H₆, 21.5-70 °C).

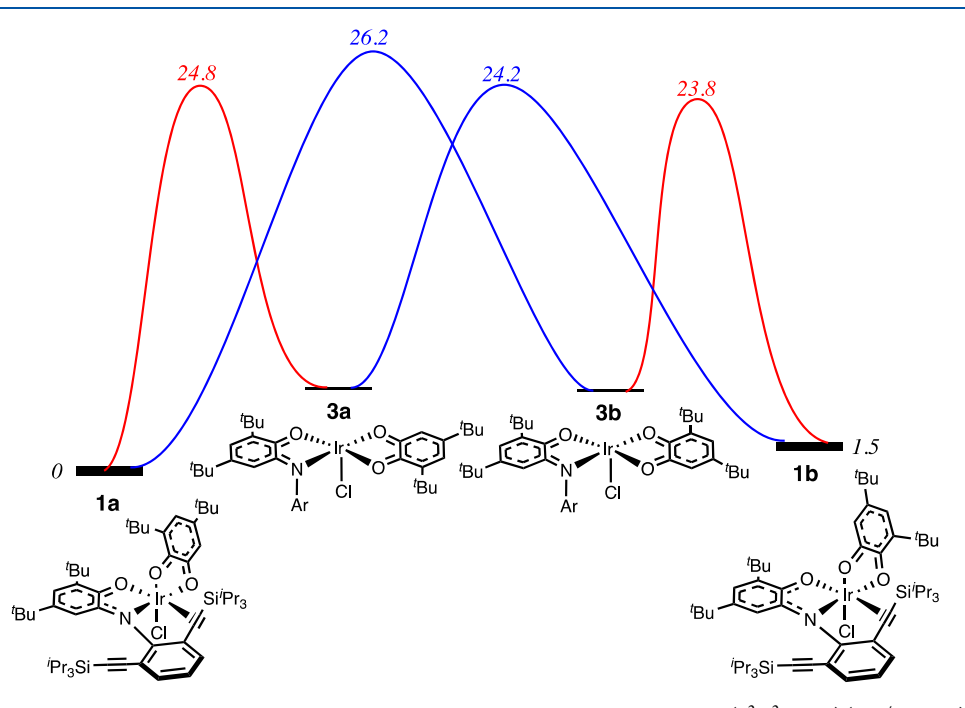


Figure 8. Experimental free energy diagram for the isomerization and pyridine addition reactions of $(\kappa^2,\eta^2\text{-Tipsi})(3,5\text{-}^4\text{Bu}_2\text{Cat})\text{IrCl}$ (benzene, 21.5 °C). Values in italics are free energies in kcal mol⁻¹ relative to 1a at 0 kcal mol⁻¹. Barriers are from pyridine additions and from the equilibration of 1a and 1b, giving a predicted $\Delta G^{\ddagger}_{1a\rightarrow 1b} = 24.9$ kcal mol⁻¹ (observed = 25.1 kcal mol⁻¹).

the value of $2.05(13) \times 10^{-5} \, \mathrm{s^{-1}}$ observed directly by 1H NMR substantiates the notion that isomerization of 1 can be entirely accounted for by a mechanism that involves alkyne dissociation.

To clarify the stereochemical aspects of the pyridine addition, we turned to DFT calculations on **1**, with the ligands simplified by replacing the triisopropylsilyl and *tert*-butyl groups with hydrogen. Simple dissociation of the alkyne

ligand in 1 would be expected to produce a square pyramid with the iminoxolene oxygen apical. This was not observed computationally because that intermediate could not be identified as a local minimum. Instead, several pathways could be identified that involved dissociation of the alkyne with an accompanying geometrical rearrangement. Square pyramidal 3, with apical chloride, can be formed directly from 1 if the dioxolene oxygen trans to Cl in 1 moves to occupy the site

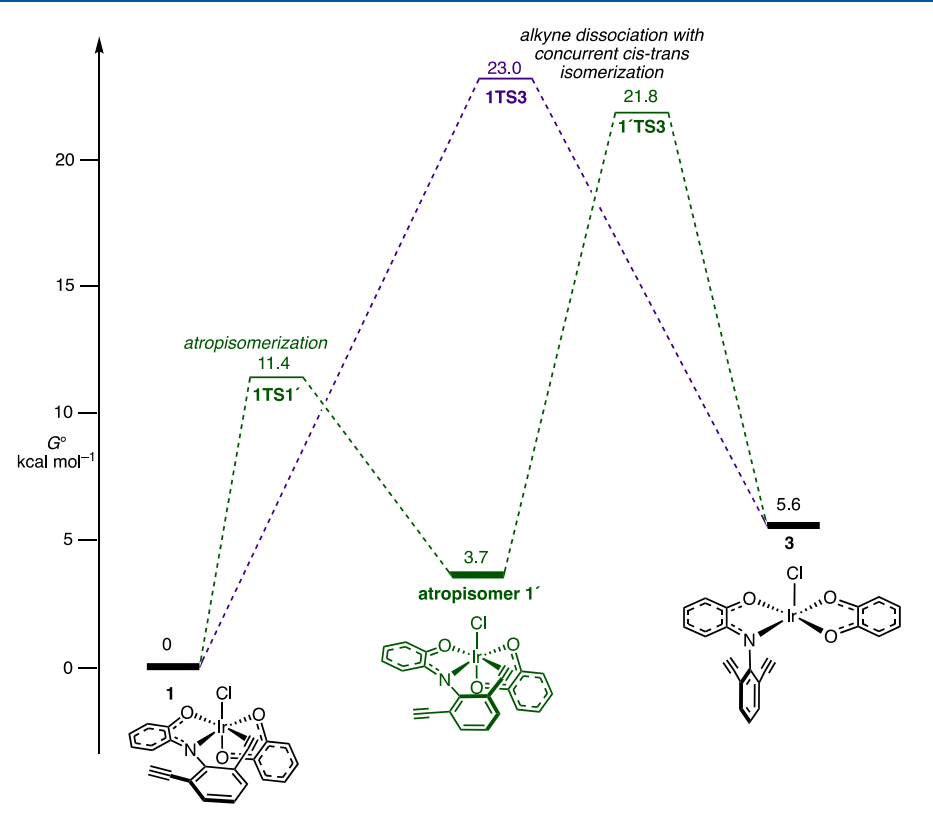


Figure 9. Calculated free energy landscape for alkyne dissociation from $(\kappa^2,\eta^2\text{-Tipsi})(\text{Cat})\text{IrCl }(1)$ to give five-coordinate 3, either directly or via initial atropisomerization. Energies in the diagram are in kcal mol⁻¹.

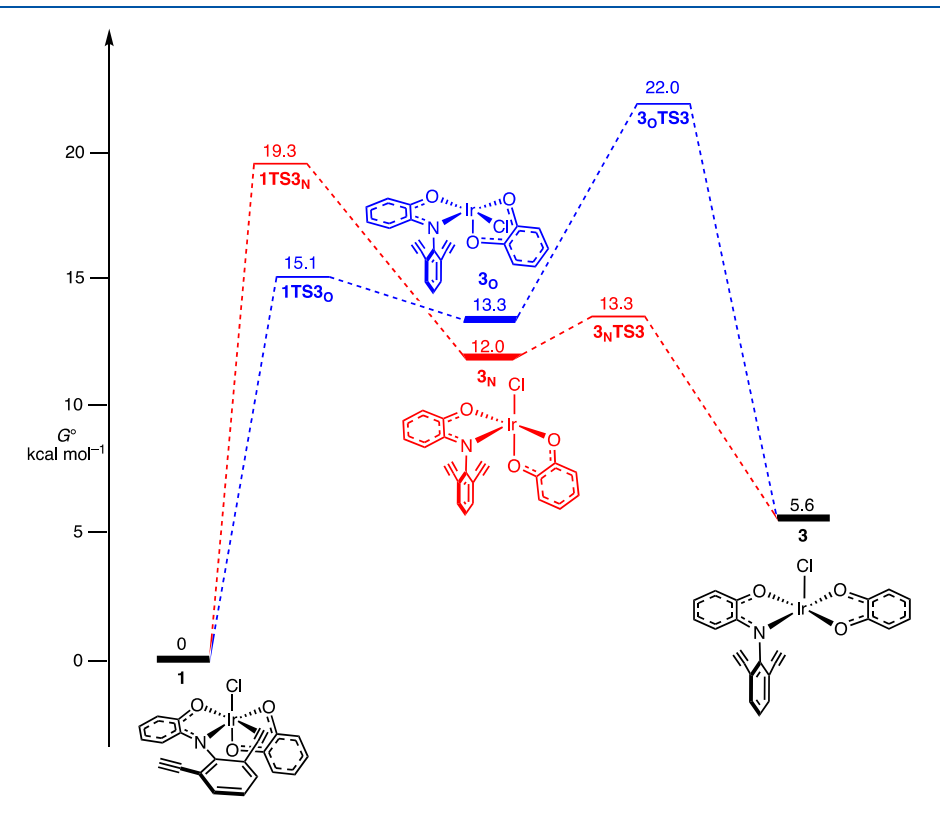


Figure 10. Calculated free energy landscape for alkyne dissociation from $(\kappa^2, \eta^2\text{-Tipsi})(\text{Cat})\text{IrCl }(1)$ to give 3 via isomeric five-coordinate intermediates 3_0 and 3_N . Energies in the diagram are in kcal mol^{-1} .

vacated by the alkyne (Figure 9, purple pathway). This pathway for alkyne loss has the highest-energy transition state of the observed possibilities. In part, this is because the free

alkyne, which is syn to chloride in 1, must move past the iminoxolene ring in this pathway, ending up anti to chloride in 3. Alternatively, atropisomerization of 1 to 1' with a modest

barrier positions the free alkyne anti to chloride prior to alkyne dissociation. Overall, the two-step pathway from 1 to 3 through atropisomer 1' (Figure 9, green pathway) is marginally more favorable kinetically than the direct (purple) pathway from 1 to 3.

Two other pathways were found to form five-coordinate intermediates isomeric to 3 (Figure 10). If the chloride swings over to displace the alkyne, a square pyramidal species with apical dioxolene oxygen ($\mathbf{3}_{O}$) is formed, while if the dioxolene oxygen initially trans to nitrogen displaces the alkyne, a five-coordinate species with apical nitrogen ($\mathbf{3}_{N}$) is formed. These two five-coordinate intermediates have the iminoxolene and dioxolene cis to each other and are calculated to be over 6 kcal mol⁻¹ less stable than the trans species 3. This is consistent with the experimentally determined structure of the five-coordinate bis(iminoxolene) complex (Diso)₂IrCl, which is square pyramidal with apical chloride. Subsequent Berry pseudorotations convert $\mathbf{3}_{N}$ and $\mathbf{3}_{O}$ to the more stable 3.

Stereochemically, the two direct pathways from 1 to 3, as well as the indirect pathway that traverses 30, retain the orientation of the tert-butyl groups of the dioxolene ($1a \rightarrow 3a$ or $1b \rightarrow 3b$), while the pathway involving 3_N switches the orientation of the tert-butyl groups $(1a \rightarrow 3b \text{ or } 1b \rightarrow 3a)$. The observed stereoselectivities would thus require the pathway via 3_N to be competitive with some combination of the three other pathways. Computationally, both pathways indeed have similar barriers. For the pathway involving 3_N, ΔG^{\ddagger} is 19.3 kcal mol⁻¹, and for the other three pathways, an effective total barrier of 21.4 kcal mol⁻¹ can be calculated (see derivation C in the SI). Calculations thus predict a preference for switching between the a and b isomers, whereas experimentally both isomers prefer to preserve the original isomer. The calculated barriers are ~5 kcal mol⁻¹ lower than the experimental barriers (Figure 8), in reasonable agreement especially given the simplified structures used in the calculations.

An interesting feature of the mechanism is the stability of 3 relative to the other five-coordinate intermediates, which appears to render 3 the stereochemical point of no return in pyridine addition. This is required by the lack of pyridine dependence of the stereoselectivity of addition and is substantiated by the complete stereospecificity of the dissociative replacement of pyridine by pyridine- d_5 in $(\kappa^2$ -Tipsi)(3,5- ${}^{t}Bu_{2}Cat$)Ir(py)Cl. The π bonding in the fivecoordinate intermediates explains why, in each pathway, the five-coordinate intermediates funnel down in energy to 3. Compared to cis isomers 3_N and 3_O, trans isomer 3 has significantly less electron density on the ligands, as demonstrated by their MOS values (Figure 11). This implies that in isomer 3, π donation from the ligands to iridium is stronger than that in 3_N or 3_O. In contrast to octahedral 1 and 2, in square pyramidal 3, the empty d_{x^2} becomes energetically accessible to accept π electrons from the ligands. A favorable interaction between the in-phase combination of ligand RAOs with the iridium d_{z^2} is evident in the calculated HOMO of 3 (Figure 11a). An analogous interaction is not possible in the cis isomers (Figure 11b,c), whose iminoxolene and dioxolene ligands are essentially nonbonding with respect to the iridium d_{z}^{2} . A π interaction similar to that proposed in isomer 3 has been described, and its spectroscopic implications noted, for (Diso)₂IrCl.¹⁸ The results of this study suggest that the energetic value of this π interaction also exerts a significant effect on the mechanism of pyridine addition to (κ^2, η^2)

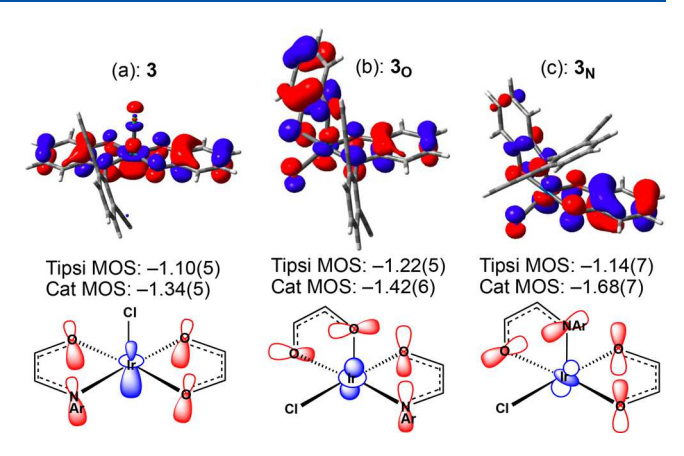


Figure 11. Kohn–Sham HOMOs, MOS values, and simplified representations of square pyramidal (κ^2 -Tipsi)(Cat)IrCl isomers: (a) 3, with apical Cl; (b) 3_O , with apical dioxolene oxygen; (c) 3_N , with apical nitrogen.

Tipsi)(3,5-^tBu₂Cat)IrCl by stabilizing the *trans* isomer 3 relative to its *cis* counterparts.

CONCLUSIONS

The preparation of a bulky iminoquinone Tipsi, which has a 2,6-di(triisopropylethynyl)phenyl substituent, enables the preparation of an octahedral iridium complex (κ^2, η^2 -Tipsi)- $(3.5^{-t}Bu_2Cat)$ IrCl, which features three different potentially π bonding ligands-iminoxolene, dioxolene, and alkynebonded to a single iridium center. Structural, spectroscopic, and computational data indicate that the iminoxolene and dioxolene are both highly engaged in π bonding with the metal center, with the strength of the former interaction somewhat stronger than that of the latter. The strength of the π interaction that these ligands experience leaves little opportunity for the alkyne to act as a π donor, and the relatively high effective oxidation state of iridium that they foster leaves little opportunity for the alkyne to act as a π acceptor. Pyridine displaces the alkyne to produce $(\kappa^2$ -Tipsi)(3,5- tBu_2 Cat)Ir(py)-Cl with little change in the structural metrics of the Tipsi and dioxolene ligands, corroborating the relative unimportance of the alkyne's π interactions. The kinetics and stereochemical aspects of the ligand substitution reaction point to a mechanism where alkyne loss competitively forms several possible square pyramidal intermediates. The intermediates with the iminoxolene and dioxolene ligands cis to each other rapidly isomerize to the square pyramidal isomer 3, with the iminoxolene and dioxolene ligands mutually trans, before 3 is trapped by pyridine. The resistance of the trans isomer 3 to further stereomutation is enforced by the opportunity for additional π bonding in the trans geometry.

■ EXPERIMENTAL SECTION

General Procedures. Unless otherwise noted, all procedures were carried out in a drybox under a nitrogen atmosphere. $[(\cos)_2 IrCl]_2$ was from Strem Chemical or prepared according to the literature procedure. The Dried solvents were purchased from Acros Organics and were stored in a nitrogen-filled drybox until use. Deuterated solvents were obtained from Cambridge Isotope Laboratories. When dry C_6D_6 was needed, it was dried over sodium and vacuum transferred away from the drying agents and stored in the drybox prior to use. NMR spectra were measured on a Bruker Avance DPX 400 or 500 MHz spectrometer. Chemical shifts for 1H and $^{13}C\{^1H\}$ spectra are reported in ppm downfield of TMS, with spectra referenced using the

known chemical shifts of the solvent residuals. Infrared spectra were recorded by ATR on a Jasco 6300 FT-IR spectrometer and are reported in wavenumbers. UV-visible-NIR spectra were recorded in 1 cm quartz cells on an Agilent 8453 diode array spectrophotometer or a Jasco V-670 spectrophotometer. Cyclic voltammograms were performed at a scan rate of 60 mV·s⁻¹ using a Metrohm Autolab PGSTAT128N potentiostat, with glassy carbon working and counter electrodes and a silver/silver chloride pseudo-reference electrode. The electrodes were connected to the potentiostat through electrical conduits in the drybox wall. Samples were 1 mM in analyte dissolved in CH₂Cl₂ with 0.1 M Bu₄NPF₆ as the electrolyte. Potentials were referenced to ferrocene/ferrocenium at 0 V.38 The reference potentials were established by spiking the test solution with a small amount of decamethylferrocene ($E^{\circ} = -0.565 \text{ V } vs \text{ Cp}_2\text{Fe}^+/\text{Cp}_2\text{Fe}$). Elemental analyses were performed by Robertson Microlit Laboratories (Ledgewood, NJ) or Midwest Microlab (Indianapolis, IN).

2,6-Bis((triisopropylsilyl)ethynyl)aniline. Into a 125 mL glass bomb are weighed 1.9861 g of 2,6-dibromoaniline (7.91 mmol), 302.1 mg of PdCl₂(PPh₃)₂ (0.43 mmol, 0.054 equiv), and 160.8 mg of CuI (0.84 mmol, 0.107 equiv). After the addition of a stirbar, the bomb is taken into the drybox. Inside the box, into a small vial is weighed 3.4350 g ${}^{i}\text{Pr}_{3}\text{SiCCH}$ (4.3 mL, ρ = 0.799 g/mL; 18.9 mmol, 2.4 equiv). The alkyne is dissolved in 15 mL of DMF and added to the bomb. To the bomb is added 50 mL of additional DMF and 2.7 mL of diisopropylamine (19.0 mmol, 2.4 equiv). The bomb is sealed with a Teflon valve, removed from the box, and placed in a 77 °C oil bath. After 66 h heating and stirring, the bomb is removed from the oil bath and the dark brown solution is allowed to cool to room temperature. The bomb is opened to the air and the solution is extracted with $3 \times$ 50 mL of hexane. The combined hexane layers are washed with 3 × 50 mL of H_2O and dried over MgSO₄. The solution is gravity filtered and the solvent is removed by rotary evaporation. This residue is taken into the drybox along with a new glass bomb containing a stir bar, 290.4 mg of PdCl₂(PPh₃)₂, and 145.2 mg of CuI. The residue is dissolved in 8 mL of DMF and added to the bomb. To the bomb is also added 35 mL more DMF, 1.000 mL of Pr₃SiCCH, and 1.000 mL of disopropylamine. The bomb is sealed, removed from the box, and placed into an 88 °C oil bath. After 51 h of further heating and stirring, the bomb is removed from the oil bath and allowed to cool to room temperature. The solution is extracted with 3 × 50 mL of hexane and the combined hexane layers are washed with 3×50 mL H₂O and then dried over MgSO₄. After evaporation of the hexane, the crude product is then separated into fractions by column chromatography, eluting with hexane and collecting the pure fractions containing the dialkynylaniline ($R_f = 0.16$). The solvent is removed from the combined pure fractions through rotary evaporation to give 0.9508 g of the desired product (2.09 mmol, 26%) as an oil that solidifies to give a pale yellow solid. ¹H NMR (CDCl₃): δ 1.17 (m, 42H, ⁱPr), 4.90 (s, 2H, NH₂), 6.61 (t, 8 Hz, 1H, Ar 4-H), 7.31 (d, 8 Hz, 2H, Ar 3,5-H). ${}^{13}C\{{}^{1}H\}$ NMR (CDCl₃): δ 11.29 (SiCH, J_{SiC} = 57 Hz), 18.73 (CH[CH₃]₂), 96.33 (C \equiv C-Si), 103.14 (Ar-C \equiv C), 107.69 (Ar 2,6-C), 116.78 (Ar 4-C), 132.75 (Ar 3,5-C), 149.75 (CNH_2) . IR: 3494 (w, ν_{NH}), 3391 (w, ν_{NH}), 2941 (s), 2872 (m) 2863 (s), 2141 (m, $\nu_{C \equiv C}$), 1906 (w), 1861 (w), 1821 (w), 1741 (w), 1697 (w), 1602 (m), 1573 (w), 1444 (s), 1384 (w), 1364 (w), 1306 (m), 1280 (w), 1253 (w), 1172 (m), 1125 (w), 1071 (m), 1018 (w), 993 (m), 923 (m), 880 (s), 789 (w), 784 (m), 738 (s), 660 (s). Anal. Calcd for C₂₈H₄₇NSi₂: C, 74.10; H, 10.44; N, 3.09. Found: C, 73.95; H, 10.10; N, 3.06.

N-(2,6-Bis(triisopropylsilylethynyl)phenyl)-4,6-di-tert-butyl-2-iminobenzoquinone, Tipsi. Into a 25 mL round-bottom flask containing 0.9846 g of 2,6-bis(triisopropylethynyl)aniline (2.17 mmol) is added 1.0676 g of 3,5-di-tert-butyl-1,2-benzoquinone (4.85 mmol, 2.2 equiv) and 10 mL of glacial acetic acid. A stirbar is added and the flask stoppered with a rubber septum. The reaction mixture is heated, with stirring, in a 65 °C oil bath for 24 h. The acetic acid is removed on the rotary evaporator, and the residue is dissolved in heptane (10 mL), which is then removed on the rotary evaporator to remove any residual CH₃COOH via its azeotrope with heptane. The residue is treated with 6 mL of hexane, which causes the

precipitation of unreacted benzoquinone, which is recovered by suction filtration (0.4812 g of recovered quinone, 2.18 mmol, 81% of excess). The filtrate from the suction filtration is then loaded onto a plug of silica gel, which is washed with hexane to remove unreacted aniline, followed by 5% ethyl acetate/hexane to elute the fastermoving red-brown band. That band is stripped down on the rotary evaporator and the residue slurried in 5 mL of methanol and suction filtered. Washing the brown solid with 2 × 5 mL of methanol and airdrying for 15 min affords 0.8607 g of Tipsi (60%). The compound is a 2:1 mixture of E and Z isomers in CDCl₃ solution. ¹H NMR (CDCl₃): δ 0.99 (s, 42H, both isomers ⁱPr), 1.07, 1.30 (s, E isomer ^tBu), 1.15, 1.23 (s, Z isomer ^tBu), 5.91 (d, 2 Hz, E isomer iminoquinone 3-H), 6.63 (d, 2 Hz, Z isomer iminoquinone 3-H), 6.91 (t, 8 Hz, Z isomer NAr 4-H), 6.93 (d, 2 Hz, 1H, both isomers iminoquinone 5-H), 6.97 (t, 8 Hz, E isomer NAr 4-H), 7.43 (d, 8 Hz, 2H, both isomers NAr 3,5-H). 13 C 1 H 13 NMR (CDCl₃): Major (E) isomer: δ 11.42 (SiCH[CH₃]₂, ${}^{1}J_{SiC}$ = 56 Hz), 18.96 (SiCH[CH₃]₂), 28.46, 29.61 (C[CH₃]₃), 35.53 (2C, C[CH₃]₃), 96.08 (C \equiv CSi, ${}^{1}J_{SiC}$ = 74 Hz), 103.29 (ArC \equiv C), 112.48, 115.02, 123.51, 132.92, 133.61, 148.57, 154.08, 144.27, 157.24, 182.44 (CO). Minor (Z) isomer: δ 11.45 (SiCH[CH₃]₂), 18.90 (SiCH[CH₃]₂), 28.59, 29.51 (C[CH₃]₃), 35.37, 35.43 ($C[CH_3]_3$), 94.73 ($C \equiv CSi$), 103.86 ($ArC \equiv C$), 109.06, 121.89, 125.32, 132.97, 134.15, 147.95, 153.18, 154.72, 158.84, 177.59 (CO). IR (evapd film): 3065 (w), 2942 (s), 2864 (s), 2149 (s, $\nu_{\rm C\equiv C}$), 1671 (m, $\nu_{\rm C=O}$), 1631 (m), 1594 (m), 1565 (w), 1463 (s), 1412 (m), 1374 (s), 1281 (m), 1268 (m), 1249 (m), 1200 (m), 1165 (w), 1072 (m), 1017 (m), 996 (m), 984 (s), 919 (w), 895 (m), 883 (s), 808 (w), 769 (m), 738 (m), 676 (s), 610 (m). UV-vis (CH_2Cl_2) : 326 nm ($\varepsilon = 10,200 \text{ L mol}^{-1} \text{ cm}^{-1}$), 404 nm (4200 L mol⁻¹ cm⁻¹). Anal. Calcd for C₄₂H₆₅NOSi₂: C, 76.88; H, 9.99; N, 2.13. Found: C, 76.82; H, 10.44; N, 2.25.

 $(\kappa^2, \eta^2$ -Tipsi)(3,5- t Bu₂Cat)lrCl (1a). Into a 20 mL scintillation vial is measured 280.7 mg of Tipsi (0.4278 mmol). This vial is then brought into the drybox. Inside the box, 187.8 mg of [(coe)₂IrCl]₂ (0.4191 mmol Ir, 0.9798 equiv) is measured into a second scintillation vial. Into that vial is pipetted 8 mL of benzene to dissolve the dimer. The iridium-containing solution is pipetted into the vial containing the Tipsi, dissolving the Tipsi. The vial is securely capped, removed from the drybox, and placed in a 61 °C oil bath. After 24 h, the vial is allowed to cool to room temperature and taken into the drybox. A solution of 92.7 mg 3,5-di-tert-butyl-1,2benzoquinone (0.421 mmol, 0.982 equiv) in 0.5 mL of benzene is added to the iridium reaction mixture. The vial is then securely capped and allowed to stand at room temperature for one week to allow for conversion from the kinetic isomer 1b to the thermodynamic isomer 1a. After a week, the vial is opened to the air, the solvent is removed through rotary evaporation, and the residue is dissolved in hexane. The solution is filtered through a plug of silica gel, eluting the desired compound with 95:5 hexane:ethyl acetate as a fast-moving dark band. The solvent is removed through rotary evaporation, and the residue is slurried with methanol and vacuum filtered through a glass frit. After washing with 3 × 5 mL of methanol and air drying for 15 min, 276.3 mg of $(\kappa^2, \eta^2$ -Tipsi)(3,5- t Bu₂Cat)IrCl as pure isomer 1a (60%) is collected. ¹H NMR (C_6D_6): δ 0.96 (m, 12H, SiCH and SiCH(CH₃)₂), 1.02 (s, 9H, ^tBu), 1.03 (br, 9H, $SiCH(CH_3)_2$), 1.05 (d, 7 Hz, 9H, $SiCH(CH_3)_2$), 1.23 (s, 9H, tBu), 1.28 (s, 9H, ^tBu), 1.29 (s, 9H, ^tBu), 1.30 (d, 8 Hz, 9H, SiCH(CH₃)₂), 1.45 (sept, 8 Hz, 3H, SiCH), 6.20 (s, 1H, Cat 4,6-H or Tipsi 3,5-H), 6.24 (t, 8 Hz, 1H, NAr 4-H), 6.76 (s, 1H, Cat 4,6-H or Tipsi 3,5-H), 7.39 (d, 2 Hz, 1H, Cat 4,6-H or Tipsi 3,5-H), 7.33 (d, 2 Hz, 1H, Cat 4,6-H or Tipsi 3,5-H), 7.43 (dd, 8, 1 Hz, 1H, NAr 3-H or 5-H), 7.52 (dd, 8, 1 Hz, 1H, NAr 3-H or 5-H). ${}^{13}C\{{}^{1}H\}$ NMR (C_6D_6): δ 11.47, (SiCH), 12.15 (SiCH), 18.55 (SiCH(CH₃)₂), 18.58 (SiCH(CH₃)₂), 18.75 (SiCH(CH₃)₂), 18.87 (SiCH(CH₃)₂), 28.41 (C(CH₃)₃), 28.48 $(C(CH_3)_3)$, 30.90 $(C(CH_3)_3)$, 31.72 $(C(CH_3)_3)$, 33.75 $(C(CH_3)_3)$, 34.00 (C(CH₃)₃), 34.52 (C(CH₃)₃), 35.10 (C(CH₃)₃), 76.37 (bound C≡CSi), 101.81 (free C≡CSi), 101.89 (ArC≡C), 102.82 (ArC≡ C), 108.12, 113.79, 114.90, 118.21, 122.48, 122.26, 128.61, 134.36, 134.59, 136.49, 139.48, 142.96, 150.22, 152.87, 159.48, 165.02 (CO), 170.16 (CO), 174.83 (CO). IR: 2957 (m), 2943 (m), 2862 (m), 2143

(w, $\nu_{C\equiv C}$ free), 1966 (w, $\nu_{C\equiv C}$ coordinated), 1582 (w), 1517 (m), 1461 (m), 1406 (w), 1382 (w), 1360 (m), 1270 (w), 1219 (m), 1162 (s), 1102 (s), 1090 (w), 1009 (m), 1006 (m), 988 (m), 910 (m), 882 (m), 857 (w), 826 (w) 794 (m), 791 (w), 740 (m), 683 (m), 663 (s). UV-vis (CH₂Cl₂): 370 nm (ε = 9600 L mol⁻¹ cm⁻¹), 420 nm (9300 L mol⁻¹ cm⁻¹), 1060 nm (7500 L mol⁻¹ cm⁻¹), 1170 nm (8700 L mol⁻¹ cm⁻¹). Cyclic voltammetry: E° = 0.45, -0.68, -1.32 V. Anal. Calcd. for C₅₆H₈₅ClIrNO₃Si₂: C, 60.29; H, 7.76; N, 1.27. Found: C, 60.95; H, 7.64; N, 1.26.

 $(\kappa^2$ -Tipsi)(3,5- t Bu₂Cat)Ir(py)Cl, Isomer 2a. In the drybox, to a 20 mL scintillation vial containing 135.7 mg of $(\kappa^2, \eta^2$ -Tipsi)-(3,5-^tBu₂Cat)IrCl (1a, 0.1229 mmol) is added 7 mL of benzene and 10.0 μ L of pyridine (0.124 mmol, 1.01 equiv). The vial is securely capped and removed from the drybox and placed into a 60 °C oil bath. After 23 h, the heated vial is removed from the oil bath and allowed to cool to room temperature. Its contents are opened to the air and the solvent is removed by rotary evaporation. The residue is dissolved in hexane and separated into fractions by column chromatography, eluting with 10:1 hexane-ethyl acetate. Two dark bands elute, with 2b eluting more rapidly ($R_f = 0.36$) and 2a more slowly ($R_f = 0.17$). Fractions containing isomer 2a are pooled into a round-bottom flask, and the solvent is removed by rotary evaporation. The residue is transferred into a vial, yielding 88.9 mg of isomer 2a of $(\kappa^2$ -Tipsi)(3,5- t Bu₂Cat)Ir(py)Cl (61%). 1 H NMR (C₆D₆): δ 0.55 (sept, 8 Hz, 3H, SiCH), 0.77 (d, 7 Hz, 9H, SiCH(CH₃)₂), 0.79 (d, 7 Hz, 9H, SiCH(CH₃)₂), 0.87 (d, 7 Hz, 9H, SiCH(CH₃)₂), 0.89 (d, 7 Hz, 9H, SiCH(CH₃)₂), 1.08 (s, 9H, ^tBu), 1.23 (br, 9H, SiCH), 1.28 (s, 9H, ^tBu), 1.74 (s, 9H, ^tBu), 1.83 (s, 9H, ^tBu), 5.34 (d, 2 Hz, 1H, Cat 4,6-H or Tipsi 3,5-H), 6.02 (dd, 8, 7 Hz, 2H, py 3,5-H), 6.16 (d, 2 Hz, 1H, Cat 4,6-H or Tipsi 3,5-H), 6.39 (tt, 8, 1 Hz, 1H, py 4-H), 6.63 (d, 2 Hz, 1H, Cat 4,6-H or Tipsi 3,5-H), 6.78 (t, 8 Hz, 1H, NAr 4-H), 7.29 (d, 2 Hz, 1H, Cat 4,6-H or Tipsi 3,5-H), 7.41 (dd, 8, 2 Hz, 1H, NAr 3- or 5-H), 7.92 (dd, 8, 2 Hz, 1H, NAr 3- or 5-H), 7.93 (dd, 7, 1 Hz, 1H, py 2,6-H). ${}^{13}C\{{}^{1}H\}$ NMR (C_6D_6) : δ 11.14 (SiCH), 11.44 (SiCH), 18.58 (SiCH(CH₃)₂), 18.65 (SiCH(CH₃)₂), 18.79 $(SiCH(CH_3)_2)$, 18.85 $(SiCH(CH_3)_2)$, 29.59 $(C(CH_3)_3)$, 29.82 $(C(CH_3)_3)$, 30.44 $(C(CH_3)_3)$, 31.76 $(C(CH_3)_3)$, 32.48 $(C(CH_3)_3)$, 33.59 (C(CH₃)₃), 34.81 (Ar-C(CH₃)₃), 35.79 (Ar-C(CH₃)₃), 96.13 $(C \equiv C)$, 101.62 $(C \equiv C)$, 103.05 $(C \equiv C)$, 103.55 $(C \equiv C)$ 109.84, 113.14, 116.85, 124.14, 127.01, 129.14, 131.27, 132.46, 133.93, 134.49, 135.87, 136.02, 137.18, 141.81, 144.63, 147.57, 153.49, 156.70, 173.81 (CO), 176.41 (CO), 195.41 (CO). IR: 2945 (m), 2862 (m), 2141 (w, $\nu_{C \equiv C}$), 1664 (w), 1610 (w), 1581 (w), 1531 (m), 1521 (m), 1454 (m), 1392 (w), 1378 (m), 1359 (m), 1323 (w), 1294 (w), 1266 (w), 1248 (w), 1214 (m), 1152 (s), 1098 (s), 1069 (m), 1023 (m), 999 (m), 976 (m), 912 (m), 882 (m), 799 (m), 796 (m), 752 (w), 728 (m), 684 (m), 707 (m), 664 (s). UV-vis (CH₂Cl₂): 503 nm (ε = 5800 L mol⁻¹ cm⁻¹), 563 (shoulder, 6800 L mol⁻¹ cm⁻¹), 619 nm (5400 L mol⁻¹ cm⁻¹), 678 (shoulder, 6700 L mol⁻¹ cm⁻¹), 990 nm (14,400 L mol⁻¹ cm⁻¹), 1171 nm (shoulder, 8400 L mol⁻¹ cm⁻¹), 1331 nm (29,400 L mol⁻¹ cm⁻¹). Cyclic voltammetry: E° = 1.27, 0.39, -0.63, -1.54 V. Anal Calcd. for $C_{61}H_{90}CIIrN_2O_3Si_2$: C, 61.92; H, 7.67; N, 2.37. Found: C, 62.28; H, 7.75; N, 2.08.

 $(\kappa^2$ -Tipsi)(3,5- t Bu₂Cat)Ir(py)Cl, Isomer 2b. The procedure for the preparation of 1a is followed, using 328.8 mg of Tipsi (0.5011 mmol) and 222.4 mg of [(coe)₂IrCl]₂ (0.4964 mmol Ir, 0.9905 equiv) through the addition of 3,5-di-tert-butyl-1,2-benzoquinone (3,5-tBu₂Cat) (110.2 mg, 0.5002 mmol, 0.9982 equiv). After the addition of benzoquinone, the reaction mixture is securely sealed and stirred for 2.5 h at room temperature. Inside the dry box, 0.200 mL of pyridine (2.47 mmol, 4.93 equiv) is then added to the bomb, which is sealed and then allowed to react in a 60 °C oil bath, with stirring, for 21 h. After cooling to room temperature and evaporation of the solvent, the residue is dissolved in hexane and chromatographed on silica gel, eluting first with hexane. After a light blue band elutes, the eluent is switched to 10:1 hexane-ethyl acetate to elute 2b as the faster-moving of two dark blue bands ($R_f = 0.36$). Fractions containing the product are tested by thin layer chromatography. Any fractions containing 2b that are impure by TLC are rechromatographed with 95:5 hexane-EtOAc, and impure 2b-containing

fractions from this column are combined and rechromatographed with 97:3 hexane-EtOAc. The pure fractions are pooled in a roundbottom flask, and the solvent is removed to yield 91.4 mg (16%) of isomer **2b** of $(\kappa^2$ -Tipsi)(3,5- t Bu₂Cat)Ir(py)Cl. 1 H NMR (C₆D₆): δ 0.56 (sept, 8 Hz, 3H, SiCH), 0.78 (d, 7 Hz, 9H, SiCH(CH₃)₂), 0.80 (d, 7 Hz, 9H, SiCH(CH₃)₂), 1.12 (d, 7 Hz, 9H, SiCH(CH₃)₂), 1.17(d, 7 Hz, 9H, SiCH(CH₃)₂), 1.22 (s, 9H, ^tBu), 1.23 (s, 9H, ^tBu), 1.24 (br, 9H, SiCH), 1.60 (s, 9H, ^tBu), 1.81 (s, 9H, ^tBu), 5.58 (d, 2 Hz, 1H, Cat 4,6-H or Tipsi 3,5-H), 5.99 (d, 2 Hz, 1H, Cat 4,6-H or Tipsi 3,5-H), 6.05 (t, 7 Hz, 2H, py 3,5-H), 6.17 (d, 2 Hz, 1H, Cat 4,6-H or Tipsi 3,5-H), 6.46 (tt, 8, 1 Hz, 1H, py 4-H), 6.69 (t, 8 Hz, 1H, NAr 4-H), 7.27 (d, 2 Hz, 1H, Cat 4,6-H or Tipsi 3,5-H), 7.45 (dd, 8, 2 Hz, 1H, NAr 3- or 5-H), 7.94 (dd, 8, 1 Hz, 1H, NAr 3- or 5-H), 8.11 (dd, 7, 1 Hz, 2H, py 2,6-H). ${}^{13}C\{{}^{1}H\}$ NMR (C_6D_6) : δ 11.18 (SiCH), 11.53 (SiCH), 18.59 (SiCH(CH_3)₂), 18.69 (SiCH(CH_3)₂), 18.87 $(SiCH(CH_3)_2)$, 18.99 $(SiCH(CH_3)_2)$, 29.73 $(C(CH_3)_3)$, 30.00 $(C(CH_3)_3)$, 31.66 $(C(CH_3)_3)$, 32.18 $(C(CH_3)_3)$, 33.41 $(C(CH_3)_3)$, 33.46 ($C(CH_3)_3$), 33.23 ($C(CH_3)_3$), 35.69 ($C(CH_3)_3$), 96.22 ($C \equiv$ C), 101.33 (C \equiv C), 103.23 (C \equiv C), 103.97 (C \equiv C), 109.79, 113.17, 118.02, 124.03, 127.29, 128.61, 130.71, 133.06, 133.94, 134.18, 136.78, 137.04, 137.23, 142.74, 144.89, 147.52, 153.55, 158.53, 174.64 (CO), 177.49 (CO), 194.90 (CO). IR: 2943 (m), 2863 (m), 2142 (w, $\nu_{C \equiv C}$), 1579 (w), 1530 (w), 1454 (m), 1379 (w), 1379 (w), 1360 (s), 1324 (w), 1252 (w), 1248 (w), 1191 (w), 1155 (s), 1101 (s), 1070 (w), 1023 (m), 998 (m), 979 (m), 910 (m), 881 (m), 852 (w), 788 (w), 750 (w), 738 (m), 676 (s). UV-vis (CH₂Cl₂): 426 (ε = 2930 L mol⁻¹ cm⁻¹), 568 nm (3780 L mol⁻¹ cm⁻¹), 618 (3700 L $\rm mol^{-1}~cm^{-1}),~667~(shoulder,~3500~L~mol^{-1}~cm^{-1}),~1030~nm~(shoulder,~10,500~L~mol^{-1}~cm^{-1}),~1175~nm~(shoulder,~12,800~L~mol^{-1}~cm^{-1})$ mol⁻¹ cm⁻¹), 1295 nm (18,400 L mol⁻¹ cm⁻¹). Cyclic voltammetry: $E^{\circ} = 1.20, 0.34, -0.69, -1.51 \text{ V. Anal Calcd. for } C_{61}H_{90}\text{ClIrN}_2\text{O}_3\text{Si}_2$: C, 61.92; H, 7.67; N, 2.37. Found: C, 62.07; H, 7.98; N, 2.32.

X-ray Crystallography. Crystals of 1a • CH₃OH and 2b • PhCH₃ • 0.5 CH₃OH were grown by vapor diffusion of methanol into a solution of each complex in toluene. Crystals were placed in inert oil before being transferred to the cold N2 stream of either a Bruker Apex II or a Bruker Kappa X8-Apex-II CCD diffractometer. The data were reduced, correcting for absorption, using the program SADABS. The structures were both solved from Patterson maps. All nonhydrogen atoms were refined anisotropically. In 2b • PhCH₃ • 0.5 CH₃OH, one triisopropylsilyl group per complex was disordered and was modeled in two orientations with 50% occupancy, with methyl groups in common between the two orientations given full occupancy. One toluene per asymmetric unit was found in the difference map and modeled explicitly. Additional diffuse electron density was modeled using the SQUEEZE routine in PLATON, 40 which found 263 electrons per unit cell in a solvent-accessible volume of 1167 Å³. The electrons were attributed to one toluene and one methanol per asymmetric unit (272 electrons per unit cell). Hydrogen atoms were placed in calculated positions with their thermal parameters tied to the isotropic thermal parameters of the atoms to which they are bonded $(1.5 \times \text{ for methyl}, 1.2 \times \text{ for all others})$. Calculations used SHELXTL (Bruker AXS), 41 with scattering factors and anomalous dispersion terms taken from the literature.4

Kinetics by Optical Spectroscopy. For each experiment, a 2 mL benzene solution of either isolated 1a, or 1b generated by the addition of 3,5-di-tert-butyl to a solution of in situ-generated (Tipsi)Ir(coe)Cl, was prepared inside the drybox by serial dilution to achieve a total iridium concentration of about 5×10^{-5} M and transferred to a quartz cuvette with a septum cap. A syringe containing an excess of pyridine (10 to 40 μ L) was inserted into the septum cap (but not yet dispensed) inside the dry box. The desired temperature for each experiment was maintained by a constant-temperature bath circulating water/ethylene glycol through a multicell transport block in the Agilent 8453 spectrophotometer. After blanking the spectrometer with a benzene-filled cuvette, the cuvette for each experiment was removed from the drybox and inserted into the cell, where it was allowed to thermally equilibrate. The syringe was then dispensed and removed from the cuvette, initiating the reaction, and optical scans were taken frequently to monitor the progress of the reaction. In each

experiment, absorbances at a wavelength corresponding to a local maximum in the reactant complex (either 420 nm or 1050 nm) as a function of time were fit to $A = A_{\infty} + (A_0 - A_{\infty}) \mathrm{e}^{-kt}$ using the program Kaleidagraph (Synergy Software, v. 5.01) to determine a rate constant.

Kinetics by ¹H NMR Spectroscopy. For the experiments used to determine the rate of isomerization from 1b to 1a and the rate of pyridine addition to 1b, isomer 1b was generated by reacting Tipsi with $[(coe)_2 IrCl_2]_2$ in C_6D_6 in a screw-cap NMR tube overnight in a 60 °C oil bath. Formation of 1b was then induced by adding 3,5-ditert-butyl-1,2-benzoquinone, and dimethyl terephthalate was added as an internal standard. For the experiment measuring the rate of pyridine addition to 1b, pyridine was added to the tube ten minutes after benzoquinone. The reactions were monitored by NMR at ambient temperature, using a relaxation delay of 60 s and measuring integrals of the signals for 1b relative to the internal standard.

To measure the rate of displacement of pyridine by pyridine- d_5 in 2a and 2b, 10–15 mg of the respective (κ^2 -Tipsi)(3,5- t Bu₂Cat)Ir-(py)Cl stereoisomer was placed in a screw-cap NMR tube and dissolved in 0.6 mL of dry C_6D_6 to which pyridine- d_5 (>15 equiv) was added. Reactions were initiated by insertion of the tube into the NMR probe preheated to 60 °C (as calibrated using the peak separation in ethylene glycol). Pseudo first-order rate constants were determined from the decay of the bound pyridine signals relative to the nonexchanging peaks of the compound (relaxation delay = 60 s).

Computational Methods. Geometry optimizations were performed on simplified structures in which *tert*-butyl and triisopropylsilyl groups were replaced with hydrogen, using density functional theory (B3LYP, SDD basis set for Ir, 6-31G* basis set for all other atoms) as implemented in the Gaussian16 suite of programs. The optimized geometries for stable species were confirmed as minima and of transition states as first-order saddle points, by the calculation of vibrational frequencies. Plots of calculated Kohn—Sham orbitals were generated using Gaussview (v. 6.0.16) with an isovalue of 0.04.

ASSOCIATED CONTENT

Supporting Information

The Supporting Information is available free of charge at https://pubs.acs.org/doi/10.1021/acs.organomet.2c00431.

NMR spectra; infrared spectra; UV-visible spectra; cyclic voltammograms; kinetics data and plots; and calculated energies and MOS values by DFT (PDF)

Cartesian coordinates of calculated structures (MOL)

Accession Codes

CCDC 2194420-2194421 contain the supplementary crystallographic data for this paper. These data can be obtained free of charge via www.ccdc.cam.ac.uk/data_request/cif, or by emailing data_request/cif, or by contacting The Cambridge Crystallographic Data Centre, 12 Union Road, Cambridge CB2 1EZ, UK; fax: +44 1223 336033.

AUTHOR INFORMATION

Corresponding Author

Seth N. Brown — Department of Chemistry and Biochemistry, University of Notre Dame, Notre Dame, Indiana 46556-5670, United States; orcid.org/0000-0001-8414-2396; Email: Seth.N.Brown.114@nd.edu

Author

David A. Haungs – Department of Chemistry and Biochemistry, University of Notre Dame, Notre Dame, Indiana 46556-5670, United States

Complete contact information is available at: https://pubs.acs.org/10.1021/acs.organomet.2c00431

Notes

The authors declare no competing financial interest.

ACKNOWLEDGMENTS

This work was supported by the US National Science Foundation (CHE-1955933). We thank Dr. Allen G. Oliver for his assistance with X-ray crystallography and Dr. Evgenii Kovrigin for his help with NMR experiments. D.A.H. acknowledges support from the Notre Dame Flatley Center for Undergraduate Scholarly Engagement.

REFERENCES

- (1) Templeton, J. L. 4-Electron Alkyne Ligands in Molybdenum(II) and Tungsten(II) Complexes. *Adv. Organomet. Chem.* **1989**, *29*, 1–100
- (2) Williams, D. S.; Schrock, R. R. Synthesis and Reactivity of a Series of Analogous Rhenium Tris(imido), Bis(imido) Alkyne, and Imido Bis(alkyne) Complexes. *Organometallics* **1993**, *12*, 1148–1160.
- (3) Conry, R. R.; Mayer, J. M. Rhenium(I) Tris(acetylene) Complexes: $Re(OR')(RC \equiv CR)_3$ and $[Re(L)(RC \equiv CR)_3]OTf$. Organometallics 1993, 12, 3179–3186.
- (4) Erickson, A. N.; Gianino, J.; Markovitz, S. J.; Brown, S. N. Amphiphilicity in Oxygen Atom Transfer Reactions of Oxobis-(iminoxolene)osmium Complexes. *Inorg. Chem.* **2021**, *60*, 4004–4014
- (5) Gianino, J.; Brown, S. N. Highly covalent metal-ligand π bonding in chelated bis- and tris(iminoxolene) complexes of osmium and ruthenium. *Dalton Trans.* **2020**, *49*, 7015–7027.
- (6) Gianino, J.; Erickson, A. N.; Markovitz, S. J.; Brown, S. N. Highvalent osmium iminoxolene complexes. *Dalton Trans.* **2020**, 49, 8504–8515.
- (7) Brown, S. N. Metrical Oxidation States of 2-Amidophenoxide and Dioxolene Ligands: Structural Signatures of Metal–Ligand π Bonding in Potentially Noninnocent Ligands. *Inorg. Chem.* **2012**, *51*, 1251–1260.
- (8) Templeton, J. L.; Ward, B. C. Carbon-13 Chemical Shifts of Alkyne Ligands as Variable Electron Donors in Monomeric Molybdenum and Tungsten Complexes. *J. Am. Chem. Soc.* **1980**, 102, 3288–3290.
- (9) Shekar, S.; Brown, S. N. Mixed amidophenolate-catecholates of molybdenum(VI). *Dalton Trans.* **2014**, *43*, 3601–3611.
- (10) Nasibipour, M.; Safaei, E.; Wojtczak, A.; Jaglicic, Z.; Galindo, A.; Masoumpour, M. S. A biradical oxo-molybdenum complex containing semiquinone and o-aminophenol benzoxazolebased ligands. *RSC Adv.* **2020**, *10*, 40853–40866.
- (11) Tsys, K. V.; Chegerev, M. G.; Pashanova, K. I.; Cherkasov, A. V.; Piskunov, A. V. Synthesis and reactivity of monomeric stannylene supported by the new tetradentate O,N,N N-chelating ligand. *Inorg. Chim. Acta* **2019**, 490, 220–226.
- (12) Saeedi, R.; Safaei, E.; Lee, Y.; Lužnik, J. Oxidation of sulfides including DBT using a new vanadyl complex of a non-innocent *o*-aminophenol benzoxazole based ligand. *Appl. Organomet. Chem.* **2018**, 33, 4781–4791.
- (13) Paw, W.; Keister, J. B.; Lake, C. L.; Churchill, M. Syntheses and Reactions with Lewis Bases of $Ru_4(CO)_8(\mu_3\text{-}O_2C_6H_2R_2)_2$ (R=H, ¹Bu) Complexes Containing 1,2-Semiquinone Ligands Which Bridge through Oxygen and $\eta^6\text{-}C_6$ Rings. Crystal Structures of $Ru_4(CO)_8(O_2C_6H_4)_2 \bullet CH_2Cl_2$, $Ru_4(CO)_8(O_2C_6H_2(^1Bu)_2)_2 \bullet 2CH_2Cl_2$, $Ru_4(CO)_8(O_2C_6H_2(^1Bu)_2)_2(py)_2$, and
- $Ru_4(CO)_7(O_2C_6H_2(^tBu)_2)_2(PhCCCO_2Et)$. Organometallics 1995, 14, 767–779. (14) Abakumov, G. A.; Druzhkov, N. O.; Kurskii, Y. A.; Shavyrin, A.

S. NMR study of products of thermal transformation of substituted N-

aryl-o-quinoneimines. Russ. Chem. Bull., Int. Ed. 2003, 52, 712–717. (15) Hansch, C.; Leo, A.; Taft, R. W. A Survey of Hammett Substituent Constants and Resonance and Field Parameters. Chem. Rev. 1991, 91, 165–195.

- (16) Abakumov, G. A.; Druzhkov, N. O.; Kurskii, Y. A.; Abakumova, L. G.; Shavyrin, A. S.; Fukin, G. K.; Poddel'skii, A. I.; Cherkasov, V. K.; Okhlopkova, L. S. Quinone imines and aminophenols as precursors of new heterocycles. *Russ. Chem. Bull., Int. Ed.* **2005**, *54*, 2571–2577.
- (17) Erickson, A. N.; Brown, S. N. Molybdenum(VI) tris-(amidophenoxide) complexes. *Dalton Trans.* **2018**, 47, 15583–15595.
- (18) Do, T. H.; Brown, S. N. Mono- and Bis(iminoxolene)iridium Complexes: Synthesis and Covalency in π Bonding. *Inorg. Chem.* **2022**, *61*, 5547–5562.
- (19) Tse, Y.-H.; Auburn, P. R.; Lever, A. B. P. The *trans-cis* isomerisation of bis(dioxolene)bis(pyridine) ruthenium complexes. *Can. J. Chem.* **1992**, *70*, 1849–1854.
- (20) Schwiebert, K. E.; Stryker, J. M. Synthesis and Isolation of Highly Reactive η^3 -Allyl Alkyne Complexes of Iridium via the Inner-Sphere η^3 -Allyl Triflate Complex $(C_5Me_5)Ir(\eta^3-C_3H_5)OTf$. Facile Conversion to Alkyne Metallacyclobutane Complexes by Nucleophilic Addition. *Organometallics* **1993**, 12, 600–602.
- (21) Steinert, P.; Werner, H. A Series of Carbonyl-, Olefin-, Alkyne-, Hydrido-, and Vinyliridium Complexes Containing Bulky Bifunctional Phosphanes *i*Pr₂PCH₂X as Ligands. *Chem. Ber./Recl.* **1997**, *130*, 1591–1603.
- (22) Lo, H. C.; Grotjahn, D. B. Selective C-C Bond Formation on the First Ketene-Alkyne Complexes. *J. Am. Chem. Soc.* **1997**, *119*, 2958-2959.
- (23) Grüger, N.; Wadepohl, H.; Gade, L. H. Iridium Complexes Containing a PNP Pincer Ligand: Syntheses, Structural Chemistry, and Bond Activations. *Eur. J. Inorg. Chem.* **2013**, 5358–5365.
- (24) Espada, M. F.; Poveda, M. L.; Carmona, E. Reactivity of a Cationic $(C_5Me_5)Ir^{III}$ -Cyclometalated Phosphine Complex with Alkynes. *Organometallics* **2014**, 33, 7164–7175.
- (25) Hübner, R.; Sarkar, B.; Fiedler, J.; Záliš, S.; Kaim, W. Metal(IV) Complexes $[M(L_{N,O,S})_2]^n$ (M = Ru, Os) of a Redox-Active o-Amidophenolate Ligand $(L_{N,O,S})^{2-}$ with Coordinating Thioether Appendix. Eur. J. Inorg. Chem. **2012**, 3569–3576.
- (26) Lever, A. B. P.; Auburn, P. R.; Dodsworth, E. S.; Haga, M.; Liu, W.; Melnik, M.; Nevin, W. A. Bis(dioxolene)(bipyridine)ruthenium Redox Series. *J. Am. Chem. Soc.* **1988**, *110*, 8076–8084.
- (27) Lange, C. W.; Pierpont, C. G. (1,5-Cyclooctadiene)bis(3,6-ditert-butylcatecholato)iridium(IV). An Organometallic Aryl Oxide Complex with a Charge-Transfer Transition at Unusually Low Energy. J. Am. Chem. Soc. 1992, 114, 6582–6583.
- (28) Marhall-Roth, T.; Brown, S. N. Redox activity and π bonding in a tripodal seven-coordinate molybdenum(VI) tris(amidophenolate). *Dalton Trans.* **2015**, 44, 677–685.
- (29) Shekar, S. Part 1: Molybdenum Amidophenolates and Catecholates for Nonclassical Oxygen Activation and Atom Transfer Reactions. Part 2: Silicon-Carbon Bond Activation in Aryloxy-Iminoquinones and Enhanced Reactivity Over Tin Analogues. Ph. D. Dissertation, University of Notre Dame, Notre Dame, IN, 2014. https://curate.nd.edu/show/9s161546d9g.
- (30) Marinelli, G.; Streib, W. E.; Huffman, J. C.; Caulton, K. G.; Gagné, M. R.; Takats, J.; Dartiguenave, M.; Chardon, C.; Jackson, S. A.; Eisenstein, O. The Origin of Structural Variety of Alkyne Complexes of d⁸ Metals. An Example of Structural Isomerism. *Polyhedron* **1990**, *9*, 1867–1881.
- (31) Marinelli, G.; Rachidi, I. E.-I.; Streib, W. E.; Eisenstein, O.; Caulton, K. G. Alkyne Hydrogenation by a Dihydrogen Complex: Synthesis and Structure of an Unusual Iridium/Butyne Complex. J. Am. Chem. Soc. 1989, 111, 2346–2347.
- (32) Geer, A. M.; Julián, A.; López, J. A.; Ciriano, M. A.; Tejel, C. Pseudo-tetrahedral Rhodium and Iridium Complexes: Catalytic Synthesis of *E*-Enynes. *Chem. Eur. J.* **2018**, 24, 17545–17556.
- (33) (a) Calabrese, J. C.; Roe, D. C.; Thorn, D. L.; Tulip, T. H. Conversion of a (Methoxymethyl)iridium(I) Acetylene Complex to a Metallacyclobutane Iridium(III) Complex. Crystal and Molecular Structures of Ir(CH₂OCH₃)(*p*-tol-C≡C-*p*-tol)(PMe₃)₃ and *fac*-Ir-[CH₂C(*p*-tol)=C(*p*-tol)]Br(PMe₃)₃. Organometallics 1984, 3, 1223–1230. (b) Grotjahn, D. B.; Hoerter, J. M.; Hubbard, J. L. Double C−

- H Activation during Functionalization of Phenyl(methyl)ketene on Iridium(I) Using Alkynes. Synthesis of 1,4-Dien-3-ones. *J. Am. Chem. Soc.* **2004**, *126*, 8866–8867. (c) Li, Y.; Chan, P. K.; Leong, W. K. C–C reductive coupling mediated by attack at a spectator ligand. *J. Organomet. Chem.* **2016**, *810*, 40–45. (d) Wilklow-Marnell, M.; Brennessel, W. W.; Jones, W. D. Unexpected Solvent Effects in the Isomerization of ^{iPr}PCPIr(η^2 -PhC=CPh) to a 1-Iridaindene. *Isr. J. Chem.* **2017**, *57*, 968–974. (e) Sasakura, K.; Okamoto, K.; Ohe, K. Incorporation of Monatomic Cations onto an Ir–Ir Bond in a Dimeric Iridium(II) Complex Having a 1,3-Diene-1,4-diyl Backbone. *Organometallics* **2018**, *37*, 2319–2324.
- (34) Capelle, B.; Dartiguenave, M.; Dartiguenave, Y.; Beauchamp, A. (Trimethylphosphine)cobalt(I) Complexes. 2. Reactivity with Diphenylacetylene: Chemical and Structural Evidence for Alkyne Ligand as Variable-Electron Donor in $[Co(MeCN)(C_2Ph_2)(PMe_3)_3]BPh_4$ and $[Co(C_2Ph_2)(PMe_3)_3]BPh_4$. J. Am. Chem. Soc. 1983, 105, 4662–4670.
- (35) Shakespeare, W. Hamlet, Act I, scene 3, line 541; Edward Blount and William and Isaac Jaggard, Publishers: London, 1623.
- (36) Fay, R. C.; Lindmark, A. F. Nuclear Magnetic Resonance Studies of Inversion and Diketonate R-Group Exchange in Dialkoxybis(β -diketonato)titanium(IV) Complexes Evidence for a Twist Mechanism. *J. Am. Chem. Soc.* **1983**, *105*, 2118–2127.
- (37) Herde, J. L.; Lambert, J. C.; Senoff, C. V.; Cushing, M. A. Cyclooctene and 1,5-Cyclooctadiene Complexes of Iridium(I). *Inorg. Synth.* **1974**, *15*, 18–20.
- (38) Connelly, N. G.; Geiger, W. E. Chemical Redox Agents for Organometallic Chemistry. *Chem. Rev.* **1996**, *96*, 877–910.
- (39) Lionetti, D.; Medvecz, A. J.; Ugrinova, V.; Quiroz-Guzman, M.; Noll, B. C.; Brown, S. N. Redox-Active Tripodal Aminetris(aryloxide) Complexes of Titanium(IV). *Inorg. Chem.* **2010**, *49*, 4687–4697.
- (40) van der Sluis, P.; Spek, A. L. BYPASS: an Effective Method for the Refinement of Crystal Structures Containing Disordered Solvent Regions. *Acta Cryst.* **1990**, *A46*, 194–201.
- (41) Sheldrick, G. M. A short history of SHELX. Acta Crystallogr., Sect. A: Found. Crystallogr. 2008, 64, 112–122.
- (42) Wilson, A. J. C.; Geist, V. International Tables for Crystallography. Volume C: Mathematical, Physical and Chemical Tables; Kluwer Academic Publishers: Dordrecht/Boston/London, 1992.
- (43) Frisch, M. J.; Trucks, G. W.; Schlegel, H. B.; Scuseria, G. E.; Robb, M. A.; Cheeseman, J. R.; Scalmani, G.; Barone, V.; Petersson, G. A.; Nakatsuji, H.; Li, X.; Caricato, M.; Marenich, A. V.; Bloino, J.; Janesko, B. G.; Gomperts, R.; Mennucci, B.; Hratchian, H. P.; Ortiz, J. V.; Izmaylov, A. F.; Sonnenberg, J. L.; Williams-Young, D.; Ding, F.; Lipparini, F.; Egidi, F.; Goings, J.; Peng, B.; Petrone, A.; Henderson, T.; Ranasinghe, D.; Zakrzewski, V. G.; Gao, J.; Rega, N.; Zheng, G.; Liang, W.; Hada, M.; Ehara, M.; Toyota, K.; Fukuda, R.; Hasegawa, J.; Ishida, M.; Nakajima, T.; Honda, Y.; Kitao, O.; Nakai, H.; Vreven, T.; Throssell, K.; Montgomery, J. A., Jr.; Peralta, J. E.; Ogliaro, F.; Bearpark, M. J.; Heyd, J. J.; Brothers, E. N.; Kudin, K. N.; Staroverov, V. N.; Keith, T. A.; Kobayashi, R.; Normand, J.; Raghavachari, K.; Rendell, A. P.; Burant, J. C.; Iyengar, S. S.; Tomasi, J.; Cossi, M.; Millam, J. M.; Klene, M.; Adamo, C.; Cammi, R.; Ochterski, J. W.; Martin, R. L.; Morokuma, K.; Farkas, O.; Foresman, J. B.; Fox, D. J.. Gaussian 16, Revision C.01; Gaussian, Inc.: Wallingford CT, 2016.